THE ASTRONOMICAL JOURNAL VOLUME 103, NUMBER 3 MARCH 1992

ANALYSIS OF STELLAR OCCULTATION DATA FOR PLANETARY ATMOSPHERES. I. MODEL FITTING, WITH APPLICATION TO PLUTO

J. L. ELLIOT
Department of Earth, Atmospheric, and Planetary Sciences, and Department of Physics, Massachusetts Institute of Technology, Cambridge, Massachusetts 02139

L. A. YOUNG
Department of Earth, Atmospheric, and Planetary Sciences, Massachusetts Institute of Technology, Cambridge, Massachusetts 02139
Received 17 June 1991; revised 24 October 1991

ABSTRACT

An analytic model for a stellar-occultation light curve has been developed for a small, spherically symmetric planetary atmosphere that includes thermal and molecular weight gradients in a region that overlies an extinction layer. This work applies to the thermal structure of the upper part of Pluto's atmosphere probed by current stellar occultation data, so the issue of whether the lower part should be modeled as an extinction layer or sharp thermal gradient is not addressed. The model can be described by two equivalent sets of parameters. One set specifies the occultation light curve in terms of signal levels, times, and time intervals. Consequently, it is the more suitable set to use for fitting the light curve. The other set specifies physical parameters of the planetary atmosphere. Equations are given for the transforming between the sets of parameters, including their errors and correlation coefficients. Detailed numerical calculations are presented for a benchmark case. In order to establish the formal errors in the model parameters expected for datasets of different quality, least-squares fitting tests are carried out on synthetic datasets with different noise levels. This model has also been fit to the KAO data from the 1988 June 9 stellar occultation by Pluto. For the case with an isothermal constraint, the fitted parameters agree with our previous isothermal analysis [Elliot *et al.*, Icarus **77**, 148 (1989)]. Fits of these data that include a temperature gradient as a free parameter yield a temperature to molecular weight ratio $T/\mu = (3.72 \pm 0.75)$ K amu^{-1} and normalized gradient $(dT/dr)/T = (-4.9 \pm 7.0) \times 10^{-4}$ km^{-1} at $r = 1250$ km. Interpretation of these results depends on the mean molecular weight of the atmosphere. The values are 60 ± 12 K and -0.029 ± 0.040 K km^{-1} for the limiting case of pure CH_4 ($\mu = 16.04$) and 104 ± 21 K and -0.051 ± 0.070 K km^{-1} for the limiting case of pure N_2 ($\mu = 28.01$). Our result is consistent with the isothermal prediction of the "methane-thermostat" model of Pluto's atmosphere [Yelle & Lunine, Nature, 339, 288 (1989)]. However, Pluto's atmosphere could be isothermal in this region at a lower temperature than the 106 K predicted by the model, if the radiative cooling occurs at a wavelength longer than the 7.8 μm band of CH_4. A summary of our current knowledge of Pluto's atmosphere and related parameters is tabulated. The ambiguity between the haze and thermal-gradient possibilities for Pluto's lower atmosphere limits the accuracy with which we now know Pluto's surface radius and bulk density. If the "haze model" is correct, then Pluto's surface radius is less than 1181 km and its bulk density is greater than 1.88 g cm^{-3}. On the other hand, if the "thermal-gradient model" is correct, then Pluto's surface radius would be 1206 ± 11 km and its density would be 1.77 ± 0.33 g cm^{-3}.

1. INTRODUCTION

With the technique of stellar occultations we can probe the atmospheres of distant bodies with remarkable spatial resolution—just a few kilometers for a body at the distance of Pluto, for example. Analysis of stellar occultation light curves for atmospheric occultations has been accomplished with two approaches: (i) fitting a model to the light curve and (ii) numerical inversion. For each we assume that the atmosphere is in hydrostatic equilibrium. As previously used, model fitting yields a mean atmospheric scale height, and inversion yields scale height as a function of altitude. Neither approach requires knowledge of the refractivity or mean molecular weight of the gases comprising the atmosphere, although these are assumed not to vary over the altitude range of interest.

Following Baum & Code's (1953) development of a model for fitting the occultation light curve of a large planet with an isothermal atmosphere, Goldsmith (1963) compared such an isothermal model to a light curve produced by a large planet that had a thermal gradient. He concluded that a thermal gradient in the atmosphere could not be determined from the shape of the occultation light curve. This result was discussed by Wasserman & Veverka (1973). French *et al.* (1978) determined errors for the occultation light curve for a large planet with an isothermal atmosphere that contains photon noise. This model has been used to fit occultation curves that contain "spikes" (Elliot & Veverka 1976), with the caveat that errors in the fitted parameters are really unknown, since the spikes do not have the same statistical properties as photon noise.

In contrast to the occultation light curves of the Jovian planets and Mars, Pluto's stellar occultation curve is almost entirely devoid of spikes (Elliot *et al.* 1989), so that the modeling approach is likely to yield meaningful results, provided that one can establish the correct model atmosphere. Modeling techniques had to be extended beyond the large-planet case for analysis of the Pluto data because Pluto's scale

height at the occultation level is nearly 5% of its radius. In the context of analyzing the Pluto occultation data, corrections for the small planet case have been developed in two ways: by numerical integration to find the refraction angle (Hubbard *et al.* 1988), and by applying a correction to the results of a large-planet, isothermal model (Elliot *et al.* 1989).

Modeling of Pluto's stellar occultation data is not without its complications, however. As can be seen from its stellar occultation light curve (see Fig. 6), Pluto's atmosphere is divided into two zones: an upper zone that is clear and a lower zone that is characterized by either (i) an extinction layer (Elliot *et al.* 1989), or (ii) a sharp thermal gradient (Eshleman 1989; Hubbard *et al.* 1990). For the upper zone—under the assumption that the dominant heating mechanism is solar absorption in the 3.3 μm CH_4 band and the dominant cooling mechanism is radiation in the 7.8 μm CH_4 band—Yelle & Lunine (1989) have established that the presence of even a small amount of CH_4 would cause the atmosphere to be isothermal in this region, with a temperature of about 106 K. Although Yelle & Lunine's model requires a thermal gradient in the lower atmosphere in order to reach the surface temperature of Pluto (Hubbard *et al.* 1990), we shall refer to it as the "methane-thermostat" model (rather than the "thermal-gradient" model), in order to avoid confusion with the discussion of thermal gradients in the other parts of the atmosphere and to distinguish it from potential models in which emission by molecular species other than CH_4 might dominate the atmospheric cooling. The choice between the extinction and thermal-gradient interpretations of the lower part of Pluto's occultation light curve remains unresolved, since it has not been established that the thermal gradient required by the methane-thermostat model would necessarily be great enough to explain the structure of the light curve.

So far, modeling of Pluto's occultation light curve has been done under the assumption that the upper part of its atmosphere is isothermal, and this analysis yields a temperature to molecular weight ratio of 4.2 ± 0.4 K/amu; from this ratio, the temperature of a pure CH_4 atmosphere would be 67 ± 6 K, and that of a pure N_2 atmosphere would be 117 ± 11 K (Elliot *et al.* 1989). Combining the temperature-to-molecular-weight ratio from the occultation analysis with the temperature of 106 K from the methane-thermostat model, Yelle & Lunine (1989) find a mean molecular weight of 25 ± 3. This would imply an atmosphere dominated by a heavier gas, such as N_2, CO, or Ar (Hubbard *et al.* 1990).

Our ignorance of fundamental properties of Pluto's atmosphere—such as the identity of its major constituent and whether an extinction layer, a sharp thermal gradient, or both exist in its lower atmosphere—prompted us to extend our analytical techniques to learn more about Pluto's atmosphere from occultation data. For example, one might be able to test the methane-thermostat model by learning whether the atmosphere corresponding to the upper part of the occultation curve is indeed isothermal, as required by the model.

In this paper we examine the fundamentals of modeling stellar-occultation data for a planetary atmosphere, with the goal of establishing whether thermal and compositional gradients can be determined for Pluto's atmosphere. As discussed above, whether the break in the KAO light curve (Elliot *et al.* 1989) corresponds to a sharp thermal gradient or extinction layer remains an open question. Hence we shall be focusing our attention on the upper part of the light curve, where the methane-thermostat model predicts that the atmosphere should be isothermal. For convenience, we model the lower part of the curve as an extinction layer, since this model fits the data well.

We assume that the atmosphere is in hydrostatic equilibrium. Our analytical procedure includes all small-planet effects that have been used previously for Pluto by Hubbard *et al.* (1988) and Elliot *et al.* (1989): (i) the variation of gravitational acceleration with radius, (ii) the concentration of stellar flux due to the "refraction shrinkage" of the planet's shadow, (iii) geometrical terms that arise when the local scale height is a significant fraction of the planet's radius, and (iv) the variation in the apparent stellar velocity perpendicular to the planetary limb. Our model also includes possible thermal and compositional gradients in the planetary atmosphere.

In order to limit the scope of this work, we have made several approximations suitable for Pluto: (i) the light received at any time comes from only one point on the planetary limb, (ii) the rotational acceleration in the atmosphere is small compared with gravity, (iii) the velocity of the planet's shadow relative to the observer is constant throughout the occultation, and (iv) the atmospheric structure is spherically symmetric. To facilitate the application of our work to other planets, however, we develop a framework that can be extended to cases for which these approximations do not apply.

Our method provides a prescription for calculating a model occultation light curve that uses power series rather than numerical integrations. The resulting expressions are more transparent to how model parameters affect the light curve and require less computing time than numerical integrations.

Following the formulation of our model and tests of its performance by fitting synthetic data, we fit it to the KAO Pluto light curve for the 1988 June 9 stellar occultation, including an upper-atmosphere thermal gradient as a free parameter. We then use these results to summarize our current understanding of Pluto's atmospheric structure and to establish constraints on Pluto's surface radius and bulk density.

2. OCCULTATION LIGHT CURVE FOR A SPHERICALLY SYMMETRIC PLANET

Since a principal goal of our work is to ascertain the effect of a thermal gradient on a stellar occultation light curve, we calculate the model light curve from first principles in order to avoid overlooking any effect of the same order as a temperature gradient. We shall restrict our derivation to those steps appropriate for the Pluto occultation of 1988 June, but we set up a framework that can be extended to more general cases in the future.

Using the geometric optics approximation, we refer to the diagram of Fig. 1, where monochromatic, parallel light rays are incident on a planetary atmosphere from the left and then encounter a spherically symmetric planet. In the observer's plane (perpendicular to the incident light rays), a radial coordinate ρ has its origin at the point of intersection of this plane and the path of the light ray that would have passed through the center of the planet. The coordinate ρ is used in two ways. We write the observer's position in the plane as a function of time, $\rho = \rho(t)$, which is determined from the geocentric planetary ephemeris and the motion of

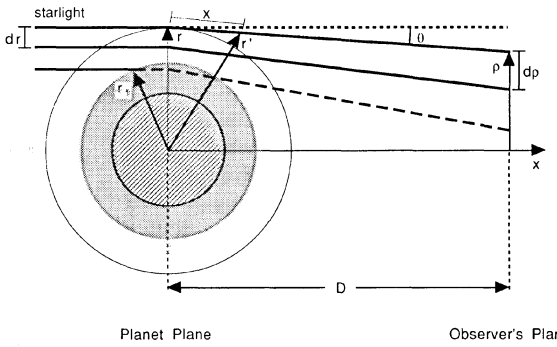

FIG. 1. Stellar occultation by a planetary atmosphere. Starlight encounters a planetary atmosphere and is bent by the gradient of refractivity in the atmosphere. Since the refraction increases exponentially with depth in the atmosphere, two neighboring rays separate by an amount proportional to distance from the planet, which causes the star to dim as seen by a distant observer. Another dimming effect is atmospheric extinction, which exists in our model only for radii less than r_1.

the observer relative to the center of the Earth. We also refer to the position in the observer's plane, $\rho = \rho(r)$, as the point of arrival for a light ray with an original path that made a closest approach r to the center of the planet.

We calculate the stellar flux in the plane of the observer by considering what happens to a bundle of light rays through their planetary encounter. The stellar flux, upon passing through the planetary atmosphere, will be changed by three effects: (i) differential bending of the light rays, (ii) absorption by the atmosphere, and (iii) partial focusing of the light by the curvature of the planetary limb in the plane perpendicular to the path of the ray. An initial bundle of light rays that has a width dr before interaction with the planet will be expanded or concentrated into a width $d\rho$ in the observer's plane, due to differential bending. The stellar flux will change by the factor $|dr/d\rho|$, where we use the absolute value so that our expression will be valid for cases when the bending of the light rays is not a monotonic function of r. Atmospheric absorption will diminish the flux by a factor $\exp[-\tau_{\rm obs}(r)]$, where $\tau_{\rm obs}(r)$ is the optical depth along the path of the ray. Finally, the focusing by the planetary limb changes the flux by the ratio of the circumferences of the "circles of light" of radius r and ρ. Hence, the flux in the observer's plane, $\zeta(r)$, is simply written as a product of three factors:

$$\zeta(r) = \frac{r}{\rho(r)} \left| \frac{dr}{d\rho(r)} \right| \exp[-\tau_{\rm obs}(r)]. \tag{2.1}$$

The singularity in $\zeta(r)$ for $\rho(r) = 0$ does not cause a problem for the analysis of the 1988 Pluto data, since none of the observations were made near the center of the shadow. For observations made near the shadow center, one can remove the singularity from the model by including effects of diffraction, the angular extent of the occulted source, and the oblateness of the planet (Elliot *et al.* 1976; 1977; 1984).

In order to evaluate the factors that appear in Eq. (2.1), we make some further assumptions. A light ray with closest approach distance r to the center of the planet is bent by the planet and then deviates from its original path by an angle $\theta(r)$. This angle lies in the plane containing the center of the planet and the original path of the ray. It is negative for rays bent toward the center of the planet, and we assume it is a small angle for the purpose of trigonometric approximations. The ray then travels to the observer's plane, lying at a distance D from the center of the planet. Since the radial coordinate ρ would never be negative, we have the following relation between the intersection points of a light ray in the two planes of interest:

$$\rho(r) = |r + D\theta(r)|. \tag{2.2}$$

We now can take the derivative needed in Eq. (2.1)

$$\left| \frac{dr}{d\rho(r)} \right| = \frac{1}{|1 + D\,[d\theta(r)/dr]|}. \tag{2.3}$$

To proceed further, we must obtain expressions for $\theta(r)$ and $\tau_{\rm obs}(r)$ in terms of the properties of the planetary atmosphere. Since our planet is spherically symmetric, its refractivity, $\nu(r')$, and linear absorption coefficient, $\kappa(r')$, are functions only of the distance from the center of the planet, r' (see Fig. 1). Since we shall need to integrate refraction and absorption along the path of the ray, we define an x coordinate that lies along the path of the ray and has its origin at the closest approach of the ray to the center of the planet. We assume that the deviation of the ray from its original path *within the atmosphere* is small enough to be neglected, so that we have the following relation between x, r, and r':

$$r'^2 = r^2 + x^2. \tag{2.4}$$

For Pluto, the effect of general relativistic bending of light can be neglected, so that the deviation of the light ray from its original path is due only to refractive gradients within the atmosphere. The refraction angle is given by the r derivative of the integral of the refractivity along the path of the ray, which we convert to a form that will prove the most useful later (Dwight 1961, Sec. 69.3):

$$\begin{aligned}\theta(r) &= \frac{d}{dr}\int_{-\infty}^{\infty} \nu[r'(x,r)]\,dx \\ &= \int_{-\infty}^{\infty} \frac{\partial \nu[r'(x,r)]}{\partial r}\,dx \\ &= \int_{-\infty}^{\infty} \frac{\partial r'}{\partial r}\frac{d\nu(r')}{dr'}\,dx \\ &= \int_{-\infty}^{\infty} \frac{r}{r'}\frac{d\nu(r')}{dr'}\,dx.\end{aligned} \tag{2.5}$$

Similarly, we find the line-of-sight optical depth by integrating the linear absorption coefficient along the path of the ray:

$$\tau_{\rm obs}(r) = \int_{-\infty}^{\infty} \kappa[r'(x,r)]\,dx. \tag{2.6}$$

In Eq. (2.1) we specified the flux as a function of the radius of closest approach to the center of the planet. To find the normalized stellar flux, $\phi(\rho)$, in the observer's plane, we add up the flux from all values of r that would arrive at ρ:

$$\phi(\rho) = \sum_{\substack{\text{perpendicular} \\ \text{limb points}}} \zeta(r). \tag{2.7}$$

Near the limb of a large planet, or planets with extinction, the light from all but the nearest limb is diminished, and only one perpendicular limb point contributes to the flux in Eq. (2.7). For the center portion of an occultation curve for a

large planet or the entire occultation curve for a small planet, light from both the near and far limbs make a significant contribution. Finally, one must consider the contributions from four perpendicular limb points within the evolute of the central flash region for oblate planets (Elliot *et al.* 1977).

The flux recorded by the observer is an integral of $\phi(\rho)$ over (i) the spectrum of the occulted star and wavelength dependent quantities in the light path, (ii) the angular distribution of source intensity, and (iii) the telescope area. For the Pluto analysis, the integrand would be constant—or at worst linear—over the range of the integration variables, so we can approximate the integrals as $\phi(\rho)$ multiplied by a constant. We represent the result as the unocculted flux of the star, $s_*(t)$, where the indicated time variability refers to the unocculted stellar flux and does not, of course, include any time variability due to the occultation. Time variability in the unocculted stellar flux could arise from intrinsic variability of the star, changes in the extinction, telescope guiding errors, or drifts in instrumental sensitivity. Similarly, we denote the background signal as $s_b(t)$, where the time variability could arise from similar causes as that for the unocculted flux from the star. Having defined these quantities, the signal, $s(t)$ that would be recorded by the observer from a position $\rho(t)$, can be written as

$$s(t) = s_*(t)\phi[\rho(t)] + s_b(t). \tag{2.8}$$

Finally, the data are integrated over a short time interval, so that our occultation dataset consists of a set of N integrations of the signal, $\{s_i\}_{i=1,\ldots,N}$, where the integrations need not be contiguous, nor of equal length. If the ith integration is centered on a time t_i, and has a length Δt_i, then the recorded signal for the ith integration, s_i can be expressed as

$$s_i = \int_{t_i - \Delta t_i/2}^{t_i + \Delta t_i/2} s(t)dt. \tag{2.9}$$

In order to express the recorded signal, $\{s_i\}_{i=1,\ldots,N}$, as an explicit function of parameters that involve the planetary atmosphere, we need an atmospheric model from which we can calculate $\theta(r)$ and $\tau_{\rm obs}(r)$; we also need to specify how to find $\rho(t)$, $s_*(t)$, and $s_b(t)$. These tasks are carried out in the next three sections: we first specify an empirical model atmosphere for the planet, then we calculate the flux in the observer's plane, and finally we combine these to find the occultation flux as a function of time.

3. EMPIRICAL MODEL FOR THE PLANETARY ATMOSPHERE

A stellar occultation light curve is shaped by refractivity gradients and extinction within the atmosphere of the occulting body. Therefore, to construct a model for the occultation light curve we require an atmospheric model for the occulting body that specifies the number density of the gas and the absorptive properties of the atmosphere. The most desirable approach would be to formulate a physical model for the atmosphere and then derive a light curve model that would be a function of the parameters of the physical model. Unfortunately our understanding of Pluto's atmosphere is insufficient at present to formulate a reliable physical model. As pointed out earlier, we lack such fundamental information as the identity of the major constituent of the atmosphere and knowledge of whether the lower part of the occultation light curve is dominated by the effect of a steep thermal gradient or an extinction layer. Hence we turn to an empirical atmospheric model.

Since a main objective of our work is to use stellar occultation data to ascertain the presence of thermal gradients, our empirical model includes a thermal gradient. A thermal gradient manifests itself in an occultation light curve as a gradient in scale height, so our model must also allow for a gradient in mean molecular weight, which could also cause a gradient in scale height. An obvious choice for the functional variation of temperature and molecular weight would be a linear expansion about a reference radius r_0, but such a formulation can lead to negative values of these quantities for large or small radii, depending on the sign of the linear coefficient. Another problem that arises with a linear formulation is that the resulting expression for the number density has an apparent singularity for a gradient of exactly zero. The singularity can be avoided by taking a limit instead of attempting a direct numerical evaluation, but this procedure introduces undesirable complexity in the computations.

An alternative functional form that does not produce negative values and is more suitable to the spherical geometry of our problem is a power law. We assume spherical symmetry and specify that the mean molecular weight is μ_0 at the reference radius r_0. We can write the mean molecular weight, $\mu(r)$ as a function of the radius r from the center of the planet and the power index a as follows:

$$\mu(r) = \mu_0 (r/r_0)^{-a}. \tag{3.1}$$

For the values of r_0 and a expected, $\mu(r)$ will be essentially a linear function over the range of interest, and the equation for the gradient of the mean molecular weight at r_0 is

$$\left.\frac{d\mu(r)}{dr}\right|_{r=r_0} = \left.\frac{-a\mu_0}{r_0}\left(\frac{r}{r_0}\right)^{-a-1}\right|_{r=r_0} = \frac{-a\mu_0}{r_0}. \tag{3.2}$$

If the temperature of the atmosphere at r_0 is T_0, we write the temperature as a function of altitude as a power law with index b:

$$T(r) = T_0\left(\frac{r}{r_0}\right)^b. \tag{3.3}$$

We have chosen opposite signs for the power indices a and b so that they both have the same sign in the ratio of temperature to molecular weight, since this ratio appears often in the subsequent derivation. The gradient of the temperature at r_0 is

$$\left.\frac{dT(r)}{dr}\right|_{r=r_0} = \left.\frac{bT_0}{r_0}\left(\frac{r}{r_0}\right)^{b-1}\right|_{r=r_0} = \frac{bT_0}{r_0}. \tag{3.4}$$

If, as a result of fitting our model to data, we find statistically significant values for the second derivatives of molecular weight or temperature, we should then become concerned about the bias introduced by our empirical model in the specification of the functional form for these quantities.

Once we allow temperature and molecular weight to become functions of radius, we must also be concerned with specifying the correct radial variation of the gravitational and centrifugal forces, so that improperly modeled radial variations in these quantities do not become aliased as variations of temperature and/or molecular weight. The r^{-2} dependence for gravity has been included in previous modeling for Pluto (Hubbard *et al.* 1988; Elliot *et al.* 1989), but the centrifugal force arising from planetary rotation has not been included—on the grounds that the ratio of centrifugal force to gravitational force at the reference radius,

$\omega^2 r_0^3/G\mathcal{M}_p$, is only 2.5×10^{-4} (G is the universal gravitational constant, $\mathcal{M}_p$ the mass of the planet, and ω the rotation rate of the atmosphere). We shall, however, include centrifugal force in our empirical atmospheric model so that it can be applied in the future to planets that have significant centrifugal forces in their atmospheres.

When planetary rotation enters the model, the planetary atmosphere becomes oblate, and spherical symmetry no longer exists. An exact solution for the occultation light curve becomes more complicated, since (i) the refractivity gradient in the atmosphere will not, in general, be coincident with the radius vector from the center of the planet, and (ii) the path of the starlight through the planetary atmosphere may sample a range of latitudes, over which the angle between the refractivity gradient and the radius vector to the center of the planet will vary. In order to avoid the problems associated with an oblate atmosphere for this paper, we formulate our model for an occultation in which the path of the starlight always lies within the equatorial plane of the planet. Although atmospheric oblateness introduced by the rotation of Pluto is not large enough to be considered in our analysis, spherical symmetry of its atmospheric structure may be violated if the atmosphere proves to be significantly oblate due to unequal heating at the poles and equator.

Having specified the radial dependences of molecular weight and temperature, we now proceed to derive an equation for the pressure of the atmosphere $p(r)$ that will be valid at the equator if the atmosphere is in hydrostatic equilibrium. If $m_{\rm amu}$ is the mass of one atomic mass unit and $n(r)$ is the number density at a radius r, then the change in pressure $dp(r)$ over an increment of radius dr must balance the sum of the gravitational and centrifugal forces on the gas within dr:

$$dp(r) = -\left(\frac{G\mathcal{M}_p}{r^2} - \omega^2 r\right)\mu(r) m_{\rm amu} n(r) dr. \tag{3.5}$$

We next write the relation between pressure, number density, Boltzmann constant k, and temperature $T(r)$ given by the perfect gas law

$$p(r) = n(r) kT(r). \tag{3.6}$$

Dividing Eq. (3.5) by Eq. (3.6), we obtain a differential equation for the pressure:

$$\frac{dp(r)}{p(r)} = -\frac{G\mathcal{M}_p \mu(r) m_{\rm amu}}{kT(r) r^2} dr + \frac{\omega^2 r \mu(r) m_{\rm amu}}{kT(r)} dr. \tag{3.7}$$

To allow the integration of the right-hand side of Eq. (3.7), we substitute the power law relations for mean molecular weight and temperature, Eqs. (3.1) and (3.3):

$$\frac{dp(r)}{p(r)} = -\frac{G\mathcal{M}_p \mu_0 m_{\rm amu}}{kT_0 r_0^2}\left(\frac{r}{r_0}\right)^{-(2+a+b)} dr + \frac{\omega^2 r_0 \mu_0 m_{\rm amu}}{kT_0}\left(\frac{r}{r_0}\right)^{1-(a+b)} dr. \tag{3.8}$$

We can consolidate most of the constants in Eq. (3.8) by defining the quantity $\lambda_g(r)$ as the ratio of the magnitude of the gravitational potential energy (referred to 0 at $r=\infty$) to kT:

$$\lambda_g(r) = \frac{G\mathcal{M}_p \mu(r) m_{\rm amu}}{kT(r) r} = \lambda_{g0}\left(\frac{r}{r_0}\right)^{-(1+a+b)}, \tag{3.9}$$

where we introduce the quantity λ_{g0} as the value of $\lambda_g(r)$ at the reference radius:

$$\lambda_{g0} \equiv \lambda_g(r_0) = \frac{G\mathcal{M}_p \mu_0 m_{\rm amu}}{kT_0 r_0}. \tag{3.10}$$

Similarly, we define the quantity $\lambda_\omega(r)$ as the ratio of the magnitude of the centrifugal potential energy (referred to 0 at $r=0$) to kT, and the value $\lambda_{\omega 0}$ and the value of $\lambda_\omega(r)$ at the reference radius:

$$\lambda_\omega(r) = \frac{\omega^2 r^2 \mu(r) m_{\rm amu}}{2kT(r)} = \lambda_{\omega 0}\left(\frac{r}{r_0}\right)^{2-(a+b)}, \tag{3.11}$$

$$\lambda_{\omega 0} \equiv \lambda_\omega(r_0) = \frac{\omega^2 r_0^2 \mu_0 m_{\rm amu}}{2kT_0}. \tag{3.12}$$

Using these, Eq. (3.8) for the pressure derivative becomes

$$\frac{dp(r)}{p(r)} = -\frac{\lambda_g(r)}{r} dr + \frac{2\lambda_\omega(r)}{r} dr = -\frac{\lambda_{g0}}{r_0}\left(\frac{r}{r_0}\right)^{-(2+a+b)} dr + \frac{2\lambda_{\omega 0}}{r_0} \times \left(\frac{r}{r_0}\right)^{1-(a+b)} dr. \tag{3.13}$$

Except when $a+b=-2$ or 1, the integral of Eq. (3.13) is given below, where we have introduced p_0 (the pressure at r_0) as a constant of integration. When $a+b=2$ or -1, then the equation will yield the correct result if we take the limit $(a+b)\to 2$ or -1.

$$p(r) = p_0 \exp\left\{\frac{\lambda_{g0}}{1+a+b}\left[\left(\frac{r}{r_0}\right)^{-(1+a+b)} - 1\right] + \frac{2\lambda_{\omega 0}}{2-(a+b)}\left[\left(\frac{r}{r_0}\right)^{2-(a+b)} - 1\right]\right\}. \tag{3.14}$$

Our next task is to find the number density. First, we define the number density at the reference radius to be n_0 and obtain its value from Eq. (3.6):

$$n_0 \equiv n(r_0) = p_0/kT_0. \tag{3.15}$$

Combining Eqs. (3.6, 3.13, and 3.14), we obtain an equation for the number density

$$n(r) = n_0\left(\frac{r}{r_0}\right)^{-b} \exp\left\{\frac{\lambda_{g0}}{1+a+b}\left[\left(\frac{r}{r_0}\right)^{-(1+a+b)} - 1\right] + \frac{2\lambda_{\omega 0}}{2-(a+b)}\left[\left(\frac{r}{r_0}\right)^{2-(a+b)} - 1\right]\right\}. \tag{3.16}$$

For bodies with "slowly rotating atmospheres" (Pluto, Triton, Titan, and Venus), the ratio of centrifugal force to gravitational force ($\omega^2 r_0^3/G\mathcal{M}_p$) is small enough to neglect the rotation term in Eq. (3.16) and still maintain adequately high precision in our model. In the interest of minimizing the complexity for the Pluto analysis carried out in this paper, we drop the rotation term here and are left with the following expression for number density:

$$n(r) = n_0\left(\frac{r}{r_0}\right)^{-b} \exp\left\{\frac{\lambda_{g0}}{1+a+b}\left[\left(\frac{r}{r_0}\right)^{-(1+a+b)} - 1\right]\right\} = n_0\left(\frac{r}{r_0}\right)^{-b} \exp\left(\frac{\lambda_g(r) - \lambda_{g0}}{1+a+b}\right). \tag{3.17}$$

Note that the final expression for the number density on the right-hand side of Eq. (3.17) reduces to that used by Elliot *et al.* (1989) and Hubbard *et al.* (1988) for the case of no thermal or molecular-weight gradients ($a = b = 0$).

The refractivity of the atmosphere as a function of radius $\nu(r)$ will depend on what gases comprise the atmosphere and their number density. If $\nu_{\rm STP}(r)$ is the refractivity of the atmospheric gas for standard conditions of temperature and pressure and L denotes Loschmidt's number, then we have

$$\nu(r) = n(r)\nu_{\rm STP}(r)/L. \tag{3.18}$$

Specifying the radial dependence of $\nu_{\rm STP}(r)$ would require some specific assumptions that would be interconnected with the radial dependence molecular weight [Eq. (3.1)]. Since these would lead us into much more detail than we can learn from the presently available Pluto stellar occultation data, especially considering the similarity of $\nu_{\rm STP}$ for the gases most likely to be in Pluto's atmosphere, we assume that $\nu_{\rm STP}(r)$ changes negligibly within the radial range of interest:

$$\nu_{\rm STP}(r) = \nu_{\rm STP}.$$

We define the refractivity at the reference radius as ν_0:

$$\nu_0 \equiv \nu(r_0) = n_0\nu_{\rm STP}/L. \tag{3.19}$$

Now we can write the equation for the refractivity for our empirical atmospheric model:

$$\nu(r) = \nu_0\left(\frac{r}{r_0}\right)^{-b}\exp\left(\frac{\lambda_g(r)-\lambda_{g0}}{1+a+b}\right). \tag{3.20}$$

Later we shall need expressions for the pressure and number density scale heights, and it is most convenient to obtain them here. The local pressure scale height $H_p(r)$ is given by

$$H_p(r) = -\left(\frac{1}{p(r)}\frac{dp(r)}{dr}\right)^{-1} = \frac{r}{\lambda_g(r)-2\lambda_\omega(r)}. \tag{3.21}$$

The number density scale height $H_n(r)$ is defined analogously to the pressure scale height. For constant $\nu_{\rm STP}$, the refractivity scale height equals the number density scale height.

$$\begin{aligned} H_n(r) &= -\left(\frac{1}{n(r)}\frac{dn(r)}{dr}\right)^{-1} \\ &= -\left(\frac{1}{p(r)}\frac{dp(r)}{dr}-\frac{1}{T(r)}\frac{dT(r)}{dr}\right)^{-1} \\ &= \frac{r}{\lambda_g(r)-2\lambda_\omega(r)+b}. \end{aligned} \tag{3.22}$$

Note that the number-density scale height equals the pressure scale height for an isothermal atmosphere ($b = 0$), and it is smaller than the pressure scale height when the temperature is increasing with altitude ($b > 0$).

In order to use our model for fitting the Pluto light curve, we must allow the lower part of the model atmosphere to have either (i) a haze layer (Elliot *et al.* 1989) or (ii) a sharp thermal gradient (Eshleman 1989; Hubbard *et al.* 1990). As discussed earlier, the correct choice has not yet been established, so for our present purpose we shall use the haze model because it is easier to implement analytically. We define the haze layer with three parameters: (i) r_1, the radius of the upper boundary of the extinction layer, (ii) κ_1, the linear absorption coefficient of the haze at r_1, and (iii) $H_{\tau 1}$, the scale height of the haze at r_1. Allowing the scale height of the haze to have the same radial dependence as gravity, we have the following equation for the linear absorption coefficient, $\kappa(r)$, of the haze:

$$\kappa(r) = \begin{cases} 0 & r > r_1, \\ \kappa_1\exp\left(-\dfrac{(r-r_1)}{H_{\tau 1}(r/r_1)}\right) & r \leqslant r_1. \end{cases} \tag{3.23}$$

This completes the specification of our empirical model atmosphere, which is summarized schematically in Fig. 2. The main results of this section are Eq. (3.20), which specifies the radial dependence of the refractivity, and Eq. (3.23), which specifies the radial dependence of the extinction.

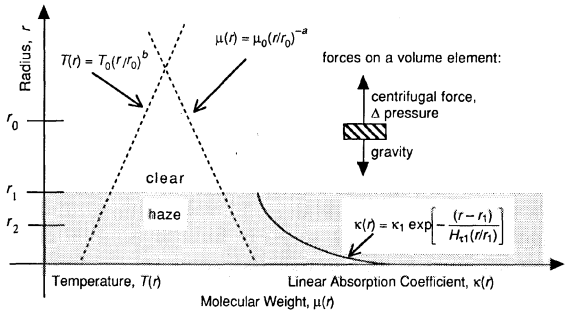

FIG. 2. Empirical model atmosphere. The temperature and mean molecular weight of the atmosphere are power law functions of the radial distance from the center of the planet, and the number density as a function of radius is derived from the assumption of hydrostatic equilibrium. An extinction layer exists in the lower part of the atmosphere, and it has a linear absorption coefficient $\kappa(r)$ that is an exponential function of radius r. This atmospheric model is used for calculating the model light curve that is used to fit the stellar occultation data.

4. STELLAR FLUX IN THE OBSERVER'S PLANE

In this section we calculate the flux received in the observer's plane given by Eq. (2.1) in terms of the empirical atmospheric model of Sec. 3. Hence equations in this and subsequent sections apply to our specific model for the atmosphere. We begin by finding the refraction angle for a light ray passing through the planetary atmosphere. Using the expression for the refractivity, $\nu(r)$, given by Eq. (3.20), we take the derivative of the refractivity required by Eq. (2.5) and express the result in terms of the energy ratios, $\lambda_g(r)$ and $\lambda_g(r')$:

$$\theta(r) = -\nu(r)\int_{-\infty}^{\infty}\left(\frac{r}{r'}\right)^{b+2} \times\exp\left(\frac{\lambda_g(r')-\lambda_g(r)}{1+a+b}\right)\frac{\lambda_g(r')+b}{r}\,dx. \tag{4.1}$$

In the large planet limit ($r \gg H_p[r]$), the integrand becomes a Gaussian, $\exp[-(x/r)^2\lambda_g(r)/2]$, equivalent to that derived by Baum & Code (1953).

Our approach to the small-planet problem is to find power series approximations in terms of the parameter $\delta \equiv 1/\lambda_g(r)$. We shall find it useful to express δ in forms involving the pressure scale height due to gravity alone, $H_{pg}(r)$, and the values of these quantities at the reference radius (λ_{g0} and H_{pg0}):

$$\delta \equiv \frac{1}{\lambda_g(r)} = \frac{1}{\lambda_{g0}} \left(\frac{r}{r_0}\right)^{1+a+b} = \frac{H_{pg}(r)}{r} = \frac{H_{pg0}}{r_0} \left(\frac{r}{r_0}\right)^{1+a+b}. \quad (4.2)$$

We note that δ becomes small in the large planet limit, but it cannot be set to zero wherever it occurs, since the planetary atmosphere will always have some finite pressure scale height that cannot be ignored on the time and distance scales of interest for the occultation light curve. Hence we have adopted the convention, for equations expressing final results, of using δ in expressions where it is added to larger terms and can be set to zero in the large planet limit. However, we use λ's and H's in those parts of the expression where these quantities should be retained in the large planet limit.

To perform the integrations in this paper, we generally use the following steps; first, factor the large planet solution out of the integral; second, change variables so that the lead term in the exponential will be Gaussian, and factor out of the integral the resulting terms that do not depend on the variable of integration; third, expand the integrand as a power series in δ; fourth, perform the integration. The result of the integration will be a power series, with a leading term of 1.

Following these steps to carry out the integration in Eq. (4.1), we first define a new variable of integration, y:

$$y = (x/r)\sqrt{1/2\delta}. \quad (4.3)$$

The integral of Eq. (4.1), expressed in terms of y, becomes

$$\theta(r) = -\nu(r)\sqrt{2\lambda_g(r)} \int_{-\infty}^{\infty} (1+2\delta y^2)^{-(2+b)/2} \times \exp\left(\frac{(1+2\delta y^2)^{-(1+a+b)/2} - 1}{(1+a+b)\delta}\right) \times [(1+2\delta y^2)^{-(1+a+b)/2} + \delta b]\, dy. \quad (4.4)$$

Expanding the integrand as a power series in δ, we obtain

$$\theta(r) = -\nu(r)\sqrt{2\lambda_g(r)} \int_{-\infty}^{\infty} e^{-y^2} \times \left\{1 + \left[b - (3+a+2b)y^2 + \left(\frac{3+a+b}{2}\right)y^4\right]\delta + O(\delta^2)\right\} dy. \quad (4.5)$$

After performing this integral, we find that $\theta(r)$ can be expressed simply as

$$\theta(r) = -\sqrt{2\pi\lambda_g(r)}\,\nu(r) A(\delta,a,b), \quad (4.6)$$

where $A(\delta,a,b)$ is a power series in δ that is given to fourth order in the Appendix, Eq. (A2). We note that $A(\delta,a,b) \to 1$ as $\delta \to 0$, so that we can set $A(\delta,a,b) = 1$ for the large-planet case.

Since $\theta(r)$ usually appears multiplied by D/r, it is convenient to have an expression for this quantity in terms of the fundamental parameters of our model. Substituting Eqs. (3.20) into (4.6), we have

$$\frac{D\theta(r)}{r} = -\frac{D\nu_0\sqrt{2\pi\lambda_{g0}}}{r_0} \left(\frac{r}{r_0}\right)^{-(3+a+3b)/2} \times \exp\left\{\frac{\lambda_{g0}}{1+a+b} \times \left[\left(\frac{r}{r_0}\right)^{-(1+a+b)} - 1\right]\right\} A(\delta,a,b). \quad (4.7)$$

Later, we shall need Eq. (4.7) evaluated at the reference radius, which is as follows:

$$\frac{D\theta_0}{r_0} = -\frac{D\nu_0\sqrt{2\pi\lambda_{g0}}}{r_0} A(\delta,a,b). \quad (4.8)$$

We shall also need the derivative of the bending angle. We calculate this by taking the derivative of Eq. (4.6) and again using a power series $B(\delta,a,b)$ that equals 1 in the limit $\delta \to 0$, Eq. (A6).

$$\frac{d\theta(r)}{dr} = \sqrt{2\pi\lambda_g^3(r)}\,\frac{\nu(r)}{r} B(\delta,a,b). \quad (4.9)$$

Expanding Eq. (4.9) and including a factor D that will be needed later we write the equation for the derivative of the refraction angle in a form similar to Eq. (4.7):

$$D\frac{d\theta(r)}{dr} = \frac{D\nu_0}{r_0}\sqrt{2\pi\lambda_{g0}^3} \left(\frac{r}{r_0}\right)^{-(5+3a+5b)/2} \times \exp\left\{\frac{\lambda_{g0}}{1+a+b} \times \left[\left(\frac{r}{r_0}\right)^{-(1+a+b)} - 1\right]\right\} B(\delta,a,b). \quad (4.10)$$

The expression for Eq. (4.10) in terms of the refraction angle is

$$D\frac{d\theta(r)}{dr} = -\frac{D\theta(r)}{r}\,\frac{\lambda_g(r) B(\delta,a,b)}{A(\delta,a,b)}. \quad (4.11)$$

The observed optical depth is related to the linear extinction coefficient by integrating along the path of the light ray through the atmosphere with closest approach r. The integral is given in Eq. (2.6) and the linear absorption coefficient is given in Eq. (3.23). Combining the two, we obtain the following expression for $\tau_{\rm obs}(r)$:

$$\tau_{\rm obs}(r) = \int_{-x_1}^{x_1} \kappa_1 \exp\left(-\frac{(r'-r_1)}{H_{\tau 1}(r'/r_1)}\right) dx, \quad (4.12)$$

where x_1 is the point on the x axis where the light ray crosses the top of the haze.

$$x_1 \equiv x(r_1) = \sqrt{r_1^2 - r^2}. \quad (4.13)$$

We perform this integration with the same procedure used for the refraction angle and its derivative. First, factor the leading terms out of the integral, so that the integrand equals 1 at $x = 0$, and rewrite the integral in $x = \sqrt{r'^2 - r^2}$.

$$\tau_{\rm obs}(r) = \kappa(r) \int_{-x_1}^{x_1} \exp\left[\frac{r_1^2}{H_{\tau 1} r}\left(\frac{1}{\sqrt{1+(x/r)^2}} - 1\right)\right] dx. \quad (4.14)$$

Once again, we change variables so that the lead term is a Gaussian. Using the haze expansion parameter $\delta_\tau \equiv H_{\tau 1} r/r_1^2$, the new variable of integration is

$$y = (x/r)\sqrt{1/2\delta_\tau}. \tag{4.15}$$

so that Eq. (4.14) becomes

$$\tau_{\rm obs}(r) = \kappa(r)\frac{r}{r_1}\sqrt{2H_{\tau 1} r} \times \int_{-y_1}^{y_1} \exp\left[\frac{1}{\delta_\tau}\left(\frac{1}{\sqrt{1+2\delta_\tau y^2}} - 1\right)\right] dy. \tag{4.16}$$

Still following the same procedure outlined for the θ integral, we expand the integrand into a Gaussian, $\exp[-y^2]$, multiplied by a power series in δ_τ.

$$\tau_{\rm obs}(r) = \kappa(r)\frac{r}{r_1}\sqrt{2H_{\tau 1} r}\int_{-y_1}^{y_1} e^{-y^2} \times \left[1 + \frac{3y^4}{2}\delta_\tau + \left(\frac{-5y^6}{2} + \frac{9y^8}{8}\right)\delta_\tau^2 + \cdots\right] dy. \tag{4.17}$$

The integration can now be performed in terms of the error function, erf, using the definite integral in Eq. (4.18), which has been derived through integration by parts and applying the definition of $\Gamma(n+1/2)$ (Dwight 1961, see Sec. 590 and Sec. 250.8):

$$\int_{-x}^{x} t^n e^{-t^2} dt = \Gamma\left(\frac{n+1}{2}\right)\mathrm{erf}(x), \tag{4.18}$$

$$\tau_{\rm obs}(r) = \kappa(r)\frac{r}{r_1}\sqrt{2\pi H_{\tau 1} r} \times \mathrm{erf}\left[\frac{r_1}{r}\left(\frac{r_1^2 - r^2}{2H_{\tau 1} r}\right)^{1/2}\right] C(\delta_\tau), \tag{4.19}$$

where $C(\delta_\tau)$ is a power series, and $C(\delta_\tau)\to 1$ for $\delta_\tau \to 0$, Eq. (A7). We expand Eq. (4.19) into a form that will be most useful for subsequent calculations:

$$\tau_{\rm obs}(r) = \begin{cases} 0 & r > r_1, \\ \kappa_1 \dfrac{r}{r_1}\sqrt{2\pi H_{\tau 1} r}\,\mathrm{erf}\left[\dfrac{r_1}{r}\left(\dfrac{r_1^2 - r^2}{2H_{\tau_1} r}\right)^{1/2}\right] \times \exp\left[-\dfrac{(r-r_1)}{H_{\tau 1}(r/r_1)}\right] C(\delta_\tau) & r \leqslant r_1. \end{cases} \tag{4.20}$$

We shall also need an expression for the optical depth in terms of the radius, r_2, at which the observed optical depth along the path of the starlight is unity. In this form we eliminate the constant κ_1 from the problem by setting the condition that the observed optical depth is 1 for $r = r_2$. For this form we shall define $\delta_{\tau 2} \equiv \delta_\tau(r_2) = H_{\tau 2}/r_2 = H_{\tau 1} r_2/r_1^2$.

$$\tau_{\rm obs}(r_2) = 1 = \kappa_1 \frac{r_2}{r_1}\sqrt{2\pi H_{\tau 1} r_2}\,\mathrm{erf}\left[\frac{r_1}{r_2}\left(\frac{r_1^2 - r_2^2}{2H_{\tau 1} r_2}\right)^{1/2}\right] \times \exp\left[-\frac{(r_2 - r_1)}{H_{\tau 1}(r_2/r_1)}\right] C(\delta_{\tau 2}). \tag{4.21}$$

We use Eq. (4.21) to eliminate κ_1 from Eq. (4.20).

$$\tau_{\rm obs}(r) = \begin{cases} 0 & r > r_1, \\ \left(\dfrac{r}{r_2}\right)^{3/2} \exp\left[\dfrac{r_1^2}{H_{\tau 1}}\left(\dfrac{1}{r} - \dfrac{1}{r_2}\right)\right] \dfrac{\mathrm{erf}\left[\dfrac{r_1}{r}\left(\dfrac{r_1^2 - r^2}{2H_{\tau 1} r}\right)^{1/2}\right] C(\delta_\tau)}{\mathrm{erf}\left[\dfrac{r_1}{r_2}\left(\dfrac{r_1^2 - r_2^2}{2H_{\tau 1} r_2}\right)^{1/2}\right] C(\delta_{\tau 2})} & r \leqslant r_1 \end{cases}. \tag{4.22}$$

For the 1988 Pluto occultation, the light-curve flux becomes negligible well before mid occultation, implying that the flux from the opposite limb can be neglected. To a good approximation, therefore, each point in the observer's plane receives stellar flux from only one radius within the planetary atmosphere, and we can use Eq. (2.2) without the absolute value bars to find $\rho(r)$:

$$\rho(r) = r + D\theta(r). \tag{4.23}$$

Then, the ratio $r/\rho(r)$, required by Eq. (2.1), is found by solving Eq. (4.23):

$$\frac{r}{\rho(r)} = \frac{1}{1 + D\theta(r)/r}. \tag{4.24}$$

In this model for Pluto we include the refracted flux from only the near limb. Thus, $\zeta(r) = \phi(r)$, and the final equation for the flux is

$$\phi(r) = \frac{\exp[-\tau_{\rm obs}(r)]}{[1 + D\,\theta(r)/r][1 + D\,d\theta(r)/dr]}. \tag{4.25}$$

The numerator and the two bracketized terms in the denominator of the right-hand side of Eq. (4.25) are obtained from Eqs. (4.7), (4.10), and (4.20).

We can now calculate the refracted stellar flux for any radius r within the planetary atmosphere with Eq. (4.25) and find the corresponding observer radius in the observer's plane, $\rho(r)$, with Eq. (4.23).

So far in this section we have assumed that the calculation proceeded with known parameters of the model atmosphere. However, we may want to leave the reference refractivity ν_0 unspecified and instead set the condition that the focused, refracted stellar flux is a specified value f at a specified radius, r_f: $\phi_{{\rm ref},f} \equiv \phi_{\rm ref}(r_f) = f$, where $0 < f < 1$, and $\phi_{\rm ref}$ refers to the refractive flux. A common choice is $f = 1/2$, for which we denote r_f by r_h (the "half-light" radius). We set up an equation for ν_f by considering the refraction terms only (no extinction) and using Eq. (4.11):

$$f = \frac{1}{\left(1 + \dfrac{D\theta(r_f)}{r_f}\right)\left(1 - \dfrac{D\theta(r_f)}{r_f}\dfrac{\lambda_{gf} B(\delta_f, a, b)}{A(\delta_f, a, b)}\right)}, \tag{4.26}$$

where $\delta_f \equiv \delta(r_f)$ and $\lambda_{gf} \equiv \lambda_g(r_f)$. If λ_{g0} and r_0 are specified, this can be solved numerically for r_f, using Eqs. (3.9) and (4.2) to find λ_{gf} and δ_f. If λ_{gf} is specified, this equation is quadratic in $D\theta(r_f)/r_f$. The positive root is taken, so that the large planet limit for the case of $f = 1/2$ is $D\theta_h/r_h = -\delta_{gh}$. The solution is

$$\frac{D\theta_f}{r_f} = \frac{1}{2}\left[\frac{A(\delta_f,a,b)}{\lambda_{gf}B(\delta_f,a,b)} - 1 + \sqrt{1+\left(2-\frac{4}{f}\right)\frac{A(\delta_f,a,b)}{\lambda_{gf}B(\delta_f,a,b)} + \left(\frac{A(\delta_f,a,b)}{\lambda_{gf}B(\delta_{gf},a,b)}\right)^2}\right]. \quad (4.27)$$

We then solve Eq. (4.6) for ν_f and substitute the expression for $D\theta(r_f)/r_f$ from Eq. (4.27) to get an equation for ν_f in terms of the radius and energy ratio at a specified flux level:

$$\nu(r_f) = \frac{r_f\left[1 - \frac{A(\delta_f,a,b)}{\lambda_{gf}B(\delta_f,a,b)} - \sqrt{1+\left(2-\frac{4}{f}\right)\frac{A(\delta_f,a,b)}{\lambda_{gf}B(\delta_f,a,b)} + \left(\frac{A(\delta_f,a,b)}{\lambda_{gf}B(\delta_f,a,b)}\right)^2}\right]}{2D\sqrt{2\pi\lambda_{gf}}A(\delta_f)}. \quad (4.28)$$

Therefore, when parameterizing the clear atmosphere, we can specify either the reference refractivity ν_0 or the reference flux level f.

5. LIGHT-CURVE MODEL

We use the term "light-curve model" to mean a prescription of calculating the stellar flux recorded by the observer as a function of time. In Sec. 4 we calculated stellar flux in terms of the radial coordinate r of the closest approach of a light ray to the occulting planet, but for a light-curve model we must be able to calculate the stellar flux in terms of the radial coordinate ρ of the observer in the observer's plane. Specification of ρ as the dependent variable introduces only one extra step in calculating the stellar flux: we first find $r(\rho)$, and then we calculate the flux with the equations in the previous section. Since our model has spherical symmetry, the angular coordinate paired with either r or ρ is of no consequence. The radii r and ρ are related by Eq. (4.23), and we solve this equation for $r(\rho)$ with Newton's method—a straightforward process, since the function is monotonic.

To complete our light-curve model, we need to find the flux for a given time $\phi(t)$. Although it would be possible to work in observer-plane coordinates, $\phi(\rho)$, the time coordinate is that for which the data are known directly. Furthermore, the integration intervals are usually evenly spaced in time, so that interpolating functions of the the model are easily formed. Calculating the model in terms of time adds another step: to find the observer's radial coordinate as a function of time, $\rho = \rho(t)$. This can be done through astrometric calculations, in which occultation chords from several stations are used to find the center of the shadow in time and space (Millis *et al.* 1992). Defining the position of the chords in the observer's plane requires some preliminary information from the light curves from each station, such as the times for a given flux level. Usually the times of half-light are used, but the times for the 0.764 flux level were used by Millis *et al.* (1992) for the Pluto case, since several stations were not sufficiently within the shadow for the flux to drop to 1/2.

A good approximation for the KAO position within Pluto's shadow for the 1988 occultation is a straight line through the shadow in the observer's plane, with a constant velocity v. If $\rho_{\min}$ is the radius at the closest approach of the observer to the center of the shadow and $t_{\rm mid}$ is the midtime of the occultation (when $\rho = \rho_{\min}$), the equation for calculating the observer's radius $\rho(t)$ is

$$\rho(t) = \sqrt{\rho_{\min}^2 + v^2(t - t_{\rm mid})^2}. \quad (5.1)$$

We emphasize that this specification for $\rho(t)$ is an adequate approximation for the KAO light curve, but one can readily calculate $\rho(t)$ with a more elaborate astrometric calculation for occultations for which nonlinear terms are significant.

Having written Eq. (5.1), we can now calculate a light curve in terms of a fundamental set of parameters, which we shall call the "atmospheric parameter set," summarized in the first column of Table 1. We have divided these parameters into four groups: (i) signal levels, (ii) geometry and data recording, (iii) clear atmosphere, and (iv) haze. From knowledge of all the parameters in this set, we can calculate an occultation light curve with equations given previously.

Now that we can calculate the model stellar flux as a function of time, we show an annotated example of such an occultation curve in Fig. 3. In anticipation of fitting this model to data, we seek an alternate set of parameters that describes the model light curve in terms of times and signal levels instead of atmospheric parameters. Of course this set of "data" parameters can be calculated from the "atmospheric" set. We have adopted the following criteria for selecting the data parameter set: they should (i) be well defined by the features in the data, (ii) have low correlations when fit to the data, (iii) be more readily comparable with other results and previously published work (such as half-light times for immersion and emersion), (iv) allow for individual fits to immersion or emersion, and (v) impose symmetry between immersion and emersion when the entire light curve is fit.

We have formulated a set of data parameters that satisfy these criteria, as illustrated in Fig. 3 and summarized in column 5 of Table 1. The parameters fall into four categories: (i) signal levels, (ii) times of events on the light curve, (iii) time scales of the refractive and extinction occultations, and (iv) parameters that affect the shape of the shoulders of the light curve.

The parameters specifying signal levels are the background level s_b, the background slope s_b', and the full scale level s_f. The first two of these comprise a linear approximation to $s_b(t)$ in Eq. (2.8). We use the midtime of the dataset $t_{\rm av}$, rather than the midtime of the occultation, as the reference time for the background slope in order to minimize the correlation of this with other model parameters. This is the average of the time of the first data point t_1 and time of the last data point t_N.

$$t_{\rm av} = (t_1 + t_N)/2, \quad (5.2)$$

$$s_b(t) = s_b + s_b'(t - t_{\rm av}). \quad (5.3)$$

The average full scale level is the sum of the star and background levels:

$$s_f = s_* + s_b. \quad (5.4)$$

Included in the choice of critical times are the immersion and emersion half-light times, $t_{\rm im}$ and $t_{\rm em}$, for the differential refraction occultation. The half-light times have been used

TABLE 1. Summary of parameter sets.

Atmospheric Parameter Set				Data Parameter Set			
Primary Member	Intermediate Quantity	Eq.	Name	Primary Member	Intermediate Quantity	Eq.	Name
Signal Levels							
s_b			background level	s_b			background level
s_b'			background slope	s_b'			background slope
s_*		(5-4)	star level	s_f		(5-4)	full-scale level
Geometry and Data Recording							
D			planet-observer distance	D			planet-observer distance
υ			shadow velocity	υ			shadow velocity
Δt			integration time	Δt			integration time
ρ_{min}		(5-8)	minimum observer radius	T_{min}		(5-8)	minimum observer radius
t_{mid}		(6-1)	midtime				
Clear Atmosphere							
a			exponent for molecular weight	a			exponent for molecular weight
b			exponent for temperature	b			exponent for temperature
r_0			reference radius	f			flux level for t_{im}, t_{em}
	ρ_h	(6-2)	half-light observer radius		r_h	(4-25)	half-light radius
	$\upsilon_{\perp,h}$	(5-9)	perpendicular velocity at ρ_h		ρ_h	(4-7)	half-light observer radius
	r_h }	(6-3)-	half-light radius		$\upsilon_{\perp,h}$	(5-9)	perpendicular velocity at ρ_h
	λ_{gh} }	(6-5)	half-light energy ratio		λ_{gh}	(6-6)	half-light energy ratio
λ_{g0}		(6-6)	reference energy ratio		H_{iso}	(5-13)	isothermal scale height
	ν_h	(4-28)	half-light refractivity	T_{Hiso}		(5-14)	refraction scale interval
ν_0		(6-7)	reference refractivity	t_{im}		(5-5)	immersion half-light time
				t_{em}		(5-5)	emersion half-light time
Haze							
$H_{\tau 1}$		(6-6)	haze scale height		r_2	(4-21)	$\tau = 1$ radius
r_1		(5-1)	top of haze	$T_{H\tau 2}$		(5-16)	haze scale interval
	r_2	(5-1)	$\tau = 1$ radius	$T_{h,2}$		(5-6)	$\tau = 1$ interval
κ_1		(6-20)	linear absorption coefficient	$T_{h,1}$		(5-7)	haze onset interval

by previous models. We choose the half-light times of immersion and emersion rather then the midtime and interval to half-light in order to easily fit immersion and emersion separately. In order to write equations for the immersion and emersion times, we first find the radius at half-light r_h. This can be found by inverting Eq. (4.25) with $f = 1/2$. Then we find the half-light radius in the observer's plane ρ_h, with Eq. (4.23). The values of t_{im} and t_{em} are given by the subsequent two solutions to Eq. (5.5), which we write by solving Eq. (5.1) for t, with the negative solution corresponding to the immersion time for a given ρ and the positive solution corresponding to the emersion time:

$$t(\rho) = t_{mid} \pm \sqrt{\rho^2 - \rho_{min}^2}/\upsilon. \tag{5.5}$$

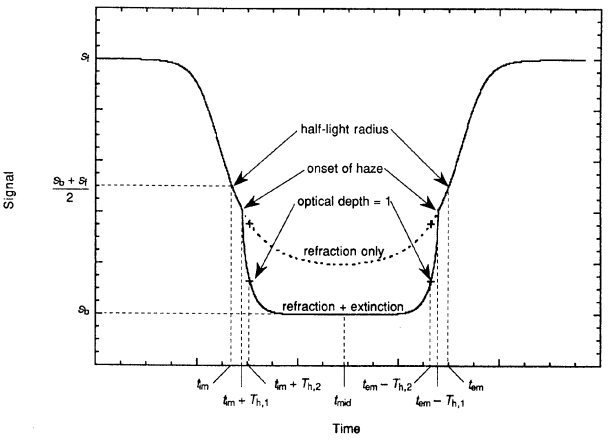

FIG. 3. Data parameters for a stellar occultation light curve. Signal level is plotted vs time for a complete occultation light curve—both immersion and emersion. In this example, the stellar flux drops to the background level s_b at midoccultation. If no extinction were present, the light curve would follow the dashed line labeled "refraction only." The times (t_{im} and t_{em}) when the stellar flux has dropped to half of its unocculted value corresponds to the "half-light" radius on the planet. The times corresponding to the onset and optical depth 1 of the haze are also indicated.

Two other light-curve parameters are the time interval between half-light and haze onset $T_{h,1}$, and the time interval between half-light and unit optical depth $T_{h,2}$. These parameters have been specified as intervals (rather than specific times) in order to impose symmetry between immersion and emersion. These time intervals are obtained from knowledge of r_h, r_1, and r_2 with Eqs. (4.23) and (5.5).

$$T_{h,1} = |t(\rho_1) - t(\rho_h)|, \tag{5.6}$$

$$T_{h,2} = |t(\rho_2) - t(\rho_h)|, \tag{5.7}$$

where $\rho_h \equiv \rho(r_h)$, $\rho_1 \equiv \rho(r_1)$, and $\rho_2 \equiv \rho(r_2)$.

In order to express all spatial coordinates as times or time intervals, scale ρ_{min} by the velocity, and use the time interval T_{min}:

$$T_{min} = \rho_{min}/\upsilon. \tag{5.8}$$

The time scale of the clear atmosphere occultation is determined by $d\phi/dt$ at half-light. Noting that $d\phi/dt = (d\phi/d\rho)(d\rho/dt)$, and that $d\rho/dt$ is the velocity of the planet perpendicular to the limb, we define the perpendicular velocity at r_h, $\upsilon_{\perp,h}$.

$$\left.\frac{d\rho}{dt}\right|_{r=r_h} \equiv \upsilon_{\perp,h} = \upsilon\frac{\sqrt{\rho_h^2 - \rho_{min}^2}}{\rho_h}. \tag{5.9}$$

The other factor in the derivative is

$$\left.\frac{d\phi}{d\rho}\right|_{r=r_h} = \frac{1}{8H_h}\left(1 + \frac{1+3a+5b}{2}\delta_h + O(\delta_h^2)\right). \tag{5.10}$$

We define the equivalent isothermal scale height $H_{\rm iso}$ as the scale height of an isothermal atmosphere with constant molecular weight that would produce a light curve with the same slope at half-light as the nonisothermal atmosphere. The relationship between H_h and $H_{\rm iso}$ is obtained by setting $a = b = 0$ in Eq. (5.11).

$$\frac{1}{8H_h}\left(1 + \frac{1+3a+5b}{2}\delta_h + \cdots\right) = \frac{1}{8H_{\rm iso}}\left(1 + \frac{1}{2}\delta_h + \cdots\right), \tag{5.11}$$

so that

$$H_{\rm iso} = \frac{H_h}{1 + [(3a+5b)/2]\delta_h + \cdots}. \tag{5.12}$$

This equation is more useful as a relation between the energy ratios:

$$\lambda_{gh} \equiv \lambda_g(r_h) = \frac{r_h}{H_{\rm iso}} - \frac{3a+5b}{2} + O(\delta_h). \tag{5.13}$$

This illustrates how the shape of a light curve for an atmosphere with a varying scale height is similar to that for a constant (but different) scale height (Goldsmith 1963). In anticipation that $H_{\rm iso}$ would be more robust in fitting than H_h, we defined our time scale of the occultation $T_{H\rm iso}$, by the scaled equivalent isothermal scale height.

$$T_{H\rm iso} = H_{\rm iso}/v_{\perp,h}. \tag{5.14}$$

Next we define an extinction scale height $H_{\tau 2}$ at the radius r_2:

$$H_{\tau 2} \equiv H_\tau(r_2) = H_{\tau 1}(r_2/r_1)^2. \tag{5.15}$$

Analogous to the procedure for refraction scale height, we scale the extinction scale height by the reference perpendicular velocity to get a time scale of the haze $T_{H\tau 2}$,

$$T_{H\tau 2} = H_{\tau 2}/v_{\perp,h}. \tag{5.16}$$

The shape of the shoulder is determined by the minimum observer radius and the exponent for temperature or molecular weight variation, b or a. The parameters a and b are used in the data parameter set with the same definitions as in the atmospheric set.

This completes our specification of the data parameter set, given in column 5 of Table 1. The equations used for converting from the atmosphere set to the data parameter set appear in column 7 of Table 1.

6. QUANTITIES DERIVED FROM FITTED PARAMETERS

We shall be fitting our light curve for the data parameter set in Table 1, but for calculating quantities that describe physical properties of the occulting atmosphere, we need to specify procedures for calculating the atmospheric parameter set from them—the inverse of the equations developed in the previous section. In this procedure, we must also calculate errors and correlation coefficients for the atmospheric parameters.

We begin with the midtime of the event, the average of the immersion and emersion half-light times:

$$t_{\rm mid} = (t_{\rm im} + t_{\rm em})/2. \tag{6.1}$$

The normalized stellar flux $\phi(\rho)$ is a function of r_0, ν_0, λ_{g0}, a, and b, as derived in Sec. 4. Often, the reference radius is specified to be half-light. However, we chose to specify our reference radius to be a value near half-light, comfortably above the haze. Since the radius of half-light will vary from occultation to occultation, we felt this was preferable. In addition, the lack of an error bar on the reference radius simplifies the propagation of errors in further calculations. To convert from $t_{\rm im}$, $t_{\rm em}$, and $T_{H\rm iso}$ to r_0, ν_0, and λ_{g0} it is useful to first calculate the half-light quantities, r_h and λ_{gh}. We start with the observer radius at half-light ρ_h.

$$\rho_h = \sqrt{\rho_{\rm min}^2 + v^2(t_{\rm em} - t_{\rm im})^2/4}, \tag{6.2}$$

which we can use to find $v_{\perp,h}$ with Eq. (5.9).

The problem of finding r_h and λ_{gh} has to be solved numerically, for which we used the method of successive substitution. The initial guess for the half-light radius is the large planet solution:

$$r_{h(1)} = \rho_h + H_{\rm iso}, \tag{6.3}$$

where $H_{\rm iso}$ is found by Eq. (5.14). In each succeeding iteration, the energy ratio for the ith iteration is found by Eq. (5.13).

$$\lambda_{gh(i)} = \frac{r_{h(i)}}{H_{\rm iso}} - \frac{3a+5b}{2}. \tag{6.4}$$

The expression $D\theta_h$ for the ith iteration is found by applying Eq. (4.26). The new half-light radius is found from the bending angle and the specified ρ_h:

$$r_{h(i+1)} = \rho_h - D\theta_h. \tag{6.5}$$

This iteration continues until $|r_{h(i+1)} - r_{h(i)}|/r_{h(i)}$ is less than a specified precision. Once the bending angle at half-light is known, the refractivity at half-light ν_h can be calculated using Eq. (4.28). The reference quantities are now

$$\lambda_{g0} = \lambda_{gh}(r_0/r_h)^{-(1+a+b)} \tag{6.6}$$

and

$$\nu_0 = \nu_h\left(\frac{r_0}{r_h}\right)^{-b}\exp\left(\frac{\lambda_{g0} - \lambda_{gh}}{1+a+b}\right). \tag{6.7}$$

With these, finding r_1 and r_2 is the standard calculation for finding $r(t)$: first find $\rho(t)$ with Eq. (5.2), then find $r(\rho)$, by solving Eq. (4.23) with Newton's method. In the data parameter set, the fitted haze scale height is defined at r_2; for the purpose of defining a quantity at a definite radius (that is independent of the occultation geometry) we convert this to the haze scale height at r_1:

$$H_{\tau 1} = T_{H\tau 2} v_{\perp,h}(r_1/r_2)^2. \tag{6.8}$$

Given r_1, r_2, and $H_{\tau 1}$, we can find κ_1 from Eq. (4.21). The preceding prescription for converting the data parameters to the atmospheric parameters is summarized in column 3 of Table 1.

To find the errors and correlations for the atmospheric set, we use the equation of error propagation from M correlated observables to M parameters (Clifford 1973). Here, the two sets of M parameters are treated as column vectors. For the dataset parameters, we define the column vector **d**,

and for the atmospheric parameters, we define the column vector **a**. The components of these vectors are the symbols in columns 1 and 5 of Table 1. The variance-covariance matrices are $\mathbf{M}_d$ and $\mathbf{M}_a$, so that $\mathbf{M}_{d,ii} = \mathrm{var}[d_i]$ and $\mathbf{M}_{d,ij} = \mathrm{cov}[d_i, d_j]$. If **B** is the derivative matrix,

$$B_{ij} = \frac{\partial a_i}{\partial d_j}, \tag{6.9}$$

then the variance-covariance matrix for the atmospheric parameters in terms of the fitted, light-curve parameters is given by the matrix equation

$$\mathbf{M}_a = \mathbf{B}\mathbf{M}_d\mathbf{B}^T, \tag{6.10}$$

where $\mathbf{B}^T$ denotes the transpose of **B**.

From these new parameters and their errors, we can find quantities of interest at half-light: the gravitational acceleration g_0, the pressure scale height H_{p0}, the ratio of temperature to molecular weight, the thermal and molecular weight gradients, and the number density and pressure:

$$g_0 = G\mathcal{M}_p/r_0^2, \tag{6.11}$$

$$H_{p0} = r_0/\lambda_0, \tag{6.12}$$

$$\frac{T_0}{\mu_0} = \frac{G\mathcal{M}_p m_{\mathrm{amu}}}{k r_0 \lambda_{g0}} = \frac{g_0 H_{p0} m_{\mathrm{amu}}}{k}, \tag{6.13}$$

$$\frac{1}{T}\frac{dT(r)}{dr}\bigg|_{r=r_0} = \frac{b}{r_0}, \tag{6.14}$$

$$\frac{1}{\mu}\frac{d\mu(r)}{dr}\bigg|_{r=r_0} = -\frac{a}{r_0}. \tag{6.15}$$

The number density at the reference radius, n_0, can be found from the refractivity at the reference radius:

$$n_0 = L(\nu_0/\nu_{\mathrm{STP}}). \tag{6.16}$$

We substitute Eq. (6.16) into the perfect gas law, Eq. (3.6), to get the pressure at the reference radius p_0:

$$p_0 = L(\nu_0/\nu_{\mathrm{STP}})kT_0. \tag{6.17}$$

Given n_0 and p_0, we use Eqs. (3.14) and (3.16) to get $n(r)$ and $p(r)$.

To find the column height above radius r, we integrate the number density from r to the top of the atmosphere, mathematically to infinity.

$$\begin{aligned}\xi(r) &= \frac{1}{L}\int_r^\infty n(r')dr' \\ &= \frac{1}{L}\int_r^\infty n_0\left(\frac{r_0}{r'}\right)^b \\ &\quad\times \exp\left\{\frac{\lambda_{g0}}{1+a+b}\left[\left(\frac{r_0}{r'}\right)^{1+a+b} - 1\right]\right\}dr'.\end{aligned} \tag{6.18}$$

In the large planet limit, the integrand is $\exp[-u]$ and the equation for the column height is $\xi(r) = H_{p0}n(r)/L$. Following the procedure in Sec. 4, we factor the large planet answer out of the integral, and perform a parameter change, so the integrand will be in the form of an exponential times a power series. In this case, the change of variables is

$$u = (r' - r)/\delta r. \tag{6.19}$$

Making the substitution and factoring $H_{p0}n(r) = \delta r n(r)$ out of the integral, the column height is

$$\begin{aligned}\xi(r) &= \frac{H_{p0}n(r)}{L}\int_0^\infty (1+\delta u)^{-b} \\ &\quad\times\exp\left(\frac{(1+\delta u)^{-(1+a+b)} - 1}{(1+a+b)\delta}\right)du.\end{aligned} \tag{6.20}$$

Once again, still following the procedure used for $\theta(r)$ and $\tau_{\mathrm{obs}}(r)$, we expand the integrand in a series in δ. As before, this integration results in a series in δ, which has a lead term of 1. The result of this is the column height, given here to second order in δ. Notice that, to first order in δ, the b dependence of $\xi(r)$ enters only in the expression for $n(r)$.

$$\begin{aligned}\xi(r) &= \frac{H_{p0}n(r)}{L}[1 + (2+a)\delta \\ &\quad + (6 + 7a + 2a^2 + 2b + ab)\delta^2 + \cdots].\end{aligned} \tag{6.21}$$

7. NUMERICAL IMPLEMENTATION OF THE LIGHT-CURVE MODEL

We have implemented our model in *Mathematica*™ version 1.2.2 (Wolfram 1988; Maeder 1990) and have carried out the numerical calculations on several Macintosh™ II series computers. This combination has 19 digits of precision for numerical calculations. For our purposes, the integrated signal [Eq. (2.9)] was well approximated by the value of the model at the midtime of the interval, except for the integration interval containing the haze onset and the adjacent integration interval corresponding to a lower level in the atmosphere. For these two cases, the model was calculated by integrating the second degree interpolating polynomials. In the bin containing the onset of the haze, two abutting polynomials were used, one for the clear portion and one for the portion with the haze. The flux was evaluated at the haze onset, the bin boundary, and the point midway between those. For the other integration interval, one polynomial was used, with model calculations at the two bin boundaries and the bin midtime.

To illustrate the appearance of light curves from planets of different radius-to-scale-height ratios, we have displayed light curves for different ratios λ_{g0} in Fig. 4. The light curves have been positioned so that their half-light times and equivalent isothermal scale heights correspond. The most striking change is the higher level of the light curves corresponding to smaller planets, due to the focusing term. If the time axis extended further, all the curves would eventually rise as times corresponding to the center of the planet were approached. However, the minimum of the light curve becomes lower for larger planets.

We show the effect of a temperature gradient on the shape of the light curve in Fig. 5, by calculating the model for different values of the temperature power index b [see Eq. (3.3)]. Note the different effect of large positive and negative values.

For the purpose of comparison with other numerical models, we present in Tables 2, 3(a), and 3(b) a benchmark case for a planet with a λ similar to Pluto's. The results of this calculation have been displayed to seven digits for different orders of the power series. Note that most of the gain from the power series is achieved with only the first term. We include the flux due to differential bending alone, ϕ_{cyl}; this is the "cylindrical-planet" approximation (Elliot *et al.* 1989, see their Appendix).

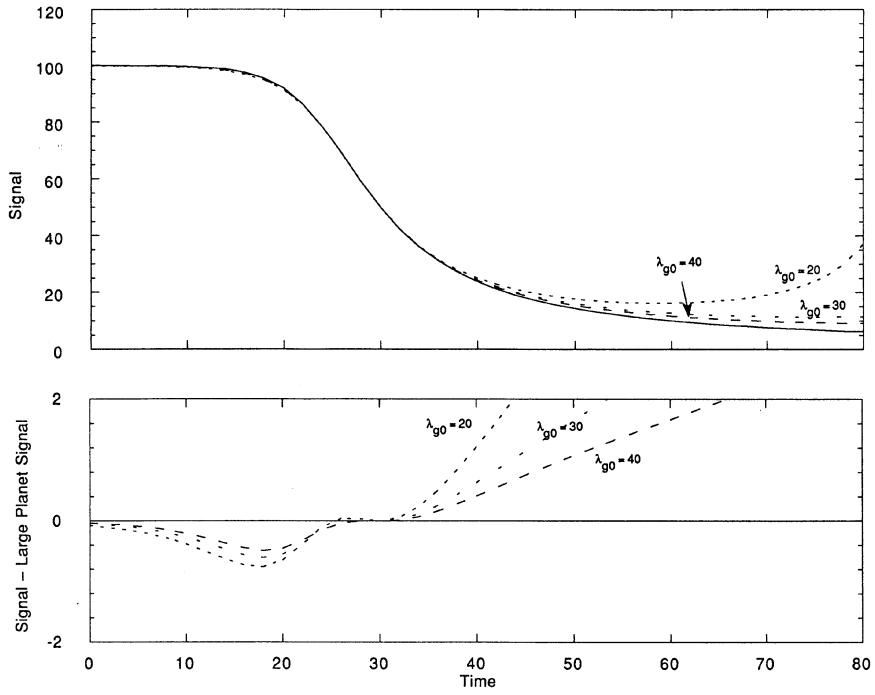

FIG. 4. Occultation light curves for small and large planets with isothermal atmospheres and no extinction. An occultation light curve for the limit of a large planet is shown by the solid line in the upper panel. The ratio of the planet's radius to its scale height is equal to λ [Eq. (3.9)]. The largest effect of a small planet is the rise in signal after the main drop, which is due to the focusing effect of the shrinking occultation shadow. For all planets, the light curve reaches a minimum at an observer radius of about half the planet radius before the focusing effect of the shrinking shadow overcomes the diminution of the light by differential refraction. The lower panel illustrates the variation in shape by showing the differences of the small planet light curves from the large planet limit, which is plotted in this panel as a horizontal line.

8. COMPARISON WITH PREVIOUS WORK

The flux equation for a large planet with no extinction has been derived for an isothermal atmosphere (Baum & Code 1953) and for an atmosphere with a linear temperature gradient (Goldsmith 1963). These models are valid near the limb of the shadow, when the atmosphere is a thin shell around the planet, as is the case for Earth, Mars, Venus, and the Jovian planets. Mathematically, their assumptions are that $\lambda_{g0} \gg 1$ and that for any r probed by the occultation, $|r - r_0| \ll r_0$. These models use a reference radius where the observed flux equals 1/2—the "half-light" radius, which we

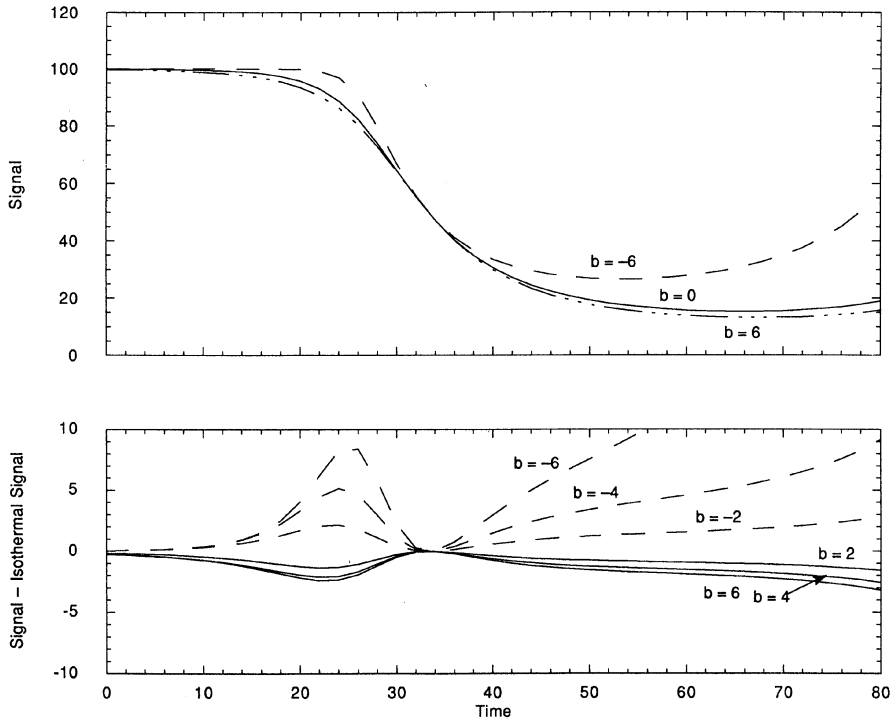

FIG. 5. Variation of the light curve due to refraction only for different values of thermal gradients. The upper panel shows an isothermal light curve and two light curves that include a thermal gradient. The lower panel shows the difference between the gradient light curves and the isothermal light curve.

TABLE 2. Parameters for benchmark model calculations.

Data Parameter	Model Value
background level, s_b (ADU)	630.000
background slope, s_b' (ADU s^{-1})	0.000
full-scale level, s_f (ADU)	3340.00
immersion half-light time, t_{im} (s*)	53.900
emersion half-light time, t_{em} (s*)	139.900
refraction scale interval, T_{Hiso} (s)	4.700
exponent for molecular weight, a	0.000
haze scale interval, $T_{h,1}$ (s)	4.200
haze onset interval, $T_{h,2}$ (s)	7.000
haze reference interval, $T_{H\tau 2}$ (s)	2.300
minimum observer radius, T_{min}, (s)†	46.900
shadow velocity, υ (km s^{-1})	18.500
integration time, Δt (s)	0.200

	$b = 0$			$b = -0.6$		
Atmospheric Parameter	0th Order	1st Order	4th Order	0th Order	1st Order	4th Order
event midtime, t_{mid} (s)	96.9	96.9	96.9	96.9	96.9	96.9
minimum observer radius, ρ_{min} (km)	867.65	867.65	867.65	867.65	867.65	867.65
refractivity at 1250, ν_0 (10^{-9})*	1.152234	1.111036	1.110238	0.9449682	1.012046	1.010128
energy ratio at 1250, λ_{g0}	21.01520	20.95764	20.95657	22.47254	22.50265	22.50100
haze onset radius, r_1 (km)	1221.175	1219.194	1219.158	1215.851	1217.324	1217.244
κ_1 (10^{-8} cm^{-1})	2.351658	2.271510	2.267495	2.313502	2.268859	2.264360
haze scale height at onset, $H_{\tau 1}$ (km)	29.28378	29.29109	29.29122	29.29941	29.29329	29.29360

*calculated for Earth-Planet distance, D = 28.89675 AU

denote by r_h. We compare our model with these two by setting our reference radius to be the half-light radius and then comparing our expression for the derivative of the flux at this radius for the large planet limit ($\delta \to 0$).

In Goldsmith's formulation, the scale height is assumed to be linear about the half-light value, $H = H_h + G(r - r_h)$, where in this section only, G is the scale-height gradient, as defined by Goldsmith (not to be confused with the gravitational constant). In terms of this notation, the flux from his Eq. (53) is

$$\phi(r) = \left[1 + \left(1 + \frac{G(r - r_h)}{H_h}\right)^{-1-(5/2)G}\right]^{-1}. \quad (8.1)$$

The derivative of (8.1) with respect to r at half-light is

$$\frac{d\phi(r)}{dr} = \frac{1 + \frac{5}{2}G}{4H_h}. \quad (8.2)$$

For the large planet case, the focusing term is not included, and Eq. (2.1) states simply that $\phi = dr/d\rho$. Thus, at half-light, $d\rho/dr = 2$ and the derivative of Goldsmith's flux with respect to the observer radius is

$$\frac{d\phi(r)}{d\rho} = \frac{1 + \frac{5}{2}G}{8H_h}. \quad (8.3)$$

Our analog to Goldsmith's G is $b\delta_h$. We compare Eq. (8.3) with Eq. (5.10) for $a = 0$, in the large-planet limit where terms of order $b\delta_h$ are retained when we take the limit $\delta_h \to 0$. They clearly give the same result. Both formulations result in the relation, for the large-planet limit,

$$H_h = H_{iso}(1 + \tfrac{5}{2}G). \quad (8.4)$$

This result differs from Goldsmith's Eq. (57), which is $H_h = H_{iso}[1 + (3/2)G]$. We have traced the discrepancy to the step between his Eqs. (55) and (56). His Eq. (55) is

$$\frac{vt}{H_{ph}} = \frac{(1/\phi - 1)\left[1 - \ln(1/\phi - 1)(1/G + \tfrac{5}{2})^{-1} + \cdots\right] - 1}{1 + \tfrac{3}{2}G} + \left(\frac{\ln(1/\phi - 1)}{1 + \frac{5}{2}G} - \cdots\right). \quad (8.5)$$

We can expand the first term on the right-hand side of Eq. (8.5) around $G = 0$ and $\phi^{-1} = 2$, and find to first order in G and $\phi^{-1} - 2$

TABLE 3(a). Benchmark model values ($b = 0.0$).

Time, t	Observer Radius, ρ	Planet Radius, r	Energy Ratio, λ_{g0}	Refractivity $\nu(r)$ (10^{-9})	$\kappa(r)$ (μm^2 cm^{-3})	Optical Depth, τ_{obs}	Unfocused Flux, ϕ_{cyl}	Refractive Flux, ϕ_{ref}	Flux, ϕ	Model Value, s_i
30.	1511.487	1512.838	17.36406	0.02991351	0.	0.	0.9847337	0.9856136	0.9856136	660.2026
		1512.774	17.31723	0.02915538	0.	0.	0.9850680	0.9859063	0.9859063	660.3612
		1512.772	17.31638	0.02914013	0.	0.	0.9850732	0.9859106	0.9859106	660.3636
35.	1436.727	1440.057	18.24164	0.07194477	0.	0.	0.9595295	0.9617532	0.9617532	647.2703
		1439.898	18.19369	0.07004203	0.	0.	0.9604435	0.9625630	0.9625630	647.7091
		1439.895	18.19282	0.07000398	0.	0.	0.9604583	0.9625758	0.9625758	647.7161
40.	1364.144	1372.513	19.13934	0.1765491	0.	0.	0.8954885	0.9009826	0.9009826	614.3326
		1372.129	19.09227	0.1720306	0.	0.	0.8976046	0.9028588	0.9028588	615.3495
		1372.122	19.09141	0.1719399	0.	0.	0.8976401	0.9028899	0.9028899	615.3663
45.	1294.104	1314.124	19.98975	0.4132307	0.	0.	0.7665589	0.7784176	0.7784176	547.9023
		1313.313	19.94730	0.4045239	0.	0.	0.7696971	0.7811222	0.7811222	549.3682
		1313.298	19.94653	0.4043444	0.	0.	0.7697511	0.7811682	0.7811682	549.3931
50.	1227.042	1268.713	20.70524	0.8451323	0.	0.	0.5952175	0.6154312	0.6154312	459.5637
		1267.368	20.67043	0.8336728	0.	0.	0.5974048	0.6170380	0.6170380	460.4346
		1267.344	20.66980	0.8334182	0.	0.	0.5974431	0.6170657	0.6170657	460.4496
55.	1163.475	1236.221	21.24944	1.456364	0.	0.	0.4443594	0.4721428	0.4721428	381.9014
		1234.434	21.22191	1.447094	0.	0.	0.4446093	0.4717257	0.4717257	381.6753
		1234.402	21.2214	1.446842	0.	0.	0.4446142	0.4717185	0.4717185	381.6714
60.	1104.005	1213.435	21.64846	2.170497	3.068288	0.7726895	0.3387185	0.3722927	0.1719134	219.1771
		1211.359	21.62616	2.168012	2.973184	0.7720796	0.3376477	0.3704808	0.1711811	218.7802
		1211.322	21.62575	2.167838	2.968097	0.7720750	0.3376299	0.3704497	0.1711675	218.7728
65.	1049.330	1197.171	21.94256	2.912644	5.426357	2.024042	0.2695612	0.3075399	0.04063229	148.0227
		1194.918	21.92373	2.919412	5.291312	2.030196	0.2678707	0.3050359	0.04005419	147.7094
		1194.877	21.92339	2.919358	5.282850	2.030242	0.2678422	0.3049932	0.04004674	147.7053
70.	1000.236	1185.307	22.16219	3.628013	8.306413	3.372716	0.2241973	0.2656800	0.009111853	130.9386
		1182.944	22.14563	3.644743	8.132926	3.391991	0.2222717	0.2628731	0.008843482	130.7932
		1182.902	22.14533	3.644822	8.120505	3.392130	0.2222394	0.2628253	0.008840642	130.7916
75.	957.5819	1176.570	22.32676	4.277044	11.42810	4.777469	0.1939656	0.2383234	0.002006034	127.0873
		1174.138	22.31173	4.303295	11.21966	4.813558	0.1919778	0.2353933	0.001911140	127.0358
		1174.094	22.31145	4.303503	11.20305	4.813811	0.1919445	0.2353437	0.001910255	127.0354
80.	922.2616	1170.204	22.44823	4.829423	14.46230	6.115231	0.1737221	0.2204258	0.0004869129	126.2639
		1167.728	22.43421	4.863993	14.22391	6.169063	0.1717401	0.2174499	0.0004551654	126.2467
		1167.683	22.43395	4.864314	14.20329	6.169427	0.1717070	0.2173997	0.0004548946	126.2466

TABLE 3(b). Benchmark model values ($b = -0.6$).

Time, t	Observer Radius, ρ	Planet Radius, r	Energy Ratio, λ_{g0}	Refractivity $\nu(r)$ (10^{-9})	$\kappa(r)$ (μm^2 cm^{-3})	Optical Depth, τ_{obs}	Unfocused Flux, ϕ_{cyl}	Refractive Flux, ϕ_{ref}	Flux, ϕ	Model Value, s_i
30.	1511.487	1512.336	20.82364	0.01717110	0.	0.	0.9884442	0.9889994	0.9889994	662.0377
		1512.366	20.85138	0.01828148	0.	0.	0.9882659	0.9888403	0.9888403	661.9514
		1512.364	20.84987	0.01825277	0.	0.	0.9882768	0.9888501	0.9888501	661.9567
35.	1436.727	1439.092	21.24128	0.04734840	0.	0.	0.9662749	0.9678653	0.9678653	650.5830
		1439.177	21.26924	0.05043916	0.	0.	0.9657168	0.9673633	0.9673633	650.3109
		1439.172	21.26771	0.05035852	0.	0.	0.9657498	0.9673930	0.9673930	650.3270
40.	1364.144	1370.731	21.65884	0.1306129	0.	0.	0.9057346	0.9101079	0.9101079	619.2785
		1370.964	21.68638	0.1390035	0.	0.	0.9042915	0.9088126	0.9088126	618.5764
		1370.951	21.68488	0.1387894	0.	0.	0.9043743	0.9088869	0.9088869	618.6167
45.	1294.104	1311.183	22.04707	0.3356766	0.	0.	0.7768944	0.7871475	0.7871475	552.6339
		1311.726	22.07295	0.3558154	0.	0.	0.7745899	0.7851374	0.7851374	551.5445
		1311.695	22.07154	0.3553466	0.	0.	0.7747185	0.7852495	0.7852495	551.6052
50.	1227.042	1264.619	22.36826	0.7332186	0.	0.	0.6007304	0.6191269	0.6191269	461.5668
		1265.575	22.39146	0.7721710	0.	0.	0.5990806	0.6178932	0.6178932	460.8981
		1265.522	22.39020	0.7714239	0.	0.	0.5991708	0.6179605	0.6179605	460.9346
55.	1163.475	1231.276	22.60862	1.315927	0.	0.	0.4454441	0.4714020	0.4714020	381.4999
		1232.587	22.62927	1.377289	0.	0.	0.4452753	0.4717253	0.4717253	381.6751
		1232.516	22.62814	1.376404	0.	0.	0.4452847	0.4717079	0.4717079	381.6657
60.	1104.005	1207.919	22.78248	2.009133	3.038130	0.7711835	0.3378478	0.3696476	0.1709492	218.6545
		1209.472	22.80128	2.093401	2.971512	0.7718181	0.3387003	0.3710567	0.1714920	218.9487
		1209.388	22.80025	2.092539	2.966026	0.7717963	0.3386551	0.3709814	0.1714610	218.9318
65.	1049.330	1191.258	22.90940	2.736507	5.449062	2.040688	0.2681358	0.3044027	0.03955388	147.4382
		1192.964	22.92697	2.842731	5.300793	2.034124	0.2694713	0.3063569	0.04006994	147.7179
		1192.872	22.92600	2.841993	5.292457	2.034348	0.2694006	0.3062530	0.04004739	147.7057
70.	1000.236	1179.104	23.00357	3.441672	8.432035	3.429558	0.2227373	0.2625684	0.008507549	130.6111
		1180.907	23.02032	3.568110	8.172710	3.408512	0.2242593	0.2647670	0.008761247	130.7486
		1180.811	23.01939	3.567539	8.161342	3.409222	0.224179	0.2646505	0.008751173	130.7431
75.	957.5819	1170.148	23.07384	4.083845	11.69941	4.892159	0.1926214	0.2353799	0.001766573	126.9575
		1172.015	23.09002	4.228142	11.31146	4.851927	0.194196	0.2376827	0.001857088	127.0065
		1171.915	23.08912	4.227748	11.29711	4.853270	0.1941131	0.2375610	0.001853645	127.0047
80.	922.2616	1163.618	23.12554	4.631788	14.90201	6.296934	0.1725127	0.2176593	0.0004009162	126.2173
		1165.527	23.14135	4.791045	14.38352	6.235892	0.1740861	0.2200049	0.0004307435	126.2335
		1165.425	23.14046	4.790814	14.36645	6.237911	0.1740033	0.2198811	0.0004296327	126.2329

TABLE 4. Scale height ratios.

Pressure Scale Height, H_{p0} (km)	Scale-Height Gradient (linear model), $G = (a + b + 2)H_{p0}/r_0$	Equivalent Isothermal Scale Height, H_{iso} (km)*	Normalized Scale-Height Ratio, $(H_{p0}/H_{iso} - 1)/G$
25	0.1	19.8	2.63
25	–0.1	33.9	2.63
25	0.3	14.4	2.45

*after Wasserman and Veverka (1973)

$$\frac{(1/\phi - 1)\left[1 - \ln(1/\phi - 1)(1/G + \tfrac{5}{2})^{-1} + \cdots\right] - 1}{1 + \tfrac{3}{2}G} = \left(\frac{1}{\phi} - 2\right)\left(1 - \frac{5}{2}G\right). \quad (8.6)$$

The second term on the right-hand side of Eq. (8.5) becomes $(1 - 5/2\ G)\ \ln(\phi^{-1} - 1)$. Substituting these results into Eq. (8.5) we have, to first order in G and $\phi^{-1} - 2$:

$$\frac{vt}{H_{ph}} = \left(1 + \frac{5}{2}\frac{b}{\lambda_{gh}}\right)^{-1} \times\left[\left(\frac{1}{\phi} - 2\right) + \ln\left(\frac{1}{\phi} - 1\right)\right] + O\left[\left(\frac{1}{\phi} - 2\right)^2\right] + O(G^2), \quad (8.7)$$

so that the correction from Goldsmith's formulation is 5/2, not 3/2, and agrees with our formulation. To determine this correction empirically, one can fit an isothermal occultation curve for a large planet (Baum & Code 1953) to a synthetic, nonisothermal curve generated by Goldsmith's (1963) equation for the flux. The empirical correction fraction, found by inverting Eq. (8.4), is $(H_h/H_{iso} - 1)/G$. Wasserman & Veverka (1973) performed such fits, and their results agree much better with a 5/2 G correction than with a 3/2 G correction. As we can see in the last column of Table 4, their results are close to our derived correction of 2.50.

9. FITS TO A SYNTHETIC LIGHT CURVE

Our next task is to fit the model described in the previous sections to synthetic data, in order to establish that the fitting is well behaved in the region of parameter values near those that apply to the KAO data. The synthetic data were generated by first calculating a model for the parameter values listed in the second column of Table 5, for midtimes ranging from 0.1 to 199.9 s (at 0.2 s intervals). Three 1000-

TABLE 5. Fits to synthetic data.

Model Parameter	Model Value	Fit #1 rms noise 2. T_{min} free	Fit #2 rms noise 2. T_{min} fixed	Fit #3 rms noise 20. T_{min} fixed	Fit #4 rms noise 200. s_b', b, T_{min} fixed
background level, s_b (ADU)	630.000	630.23 ± 0.72	630.40 ± 0.68	635.8 ± 7.5	557 ± 79
background slope, s_b' (ADU s^{-1})	0.000	0.0005 ± 0.0012	0.0005 ± 0.0012	0.015 ± 0.011	0.000
full-scale level, s_f (ADU)	3340.00	3338.96 ± 0.64	3339.08 ± 0.62	3334.3 ± 6.3	3363 ± 55
immersion half-light time, t_{im} (s*)	53.900	53.879 ± 0.019	53.872 ± 0.017	53.87 ± 0.17	52.6 ± 1.5
emersion half-light time, t_{em} (s*)	139.900	139.911 ± 0.019	139.917 ± 0.017	139.79 ± 0.17	141.8 ± 1.5
refraction scale interval, T_{Hiso} (s)	4.700	4.68 ± 0.05	4.69 ± 0.02	4.73 ± 0.18	4.28 ± 0.89
exponent for molecular weight, a	0.000	0.000	0.000	0.000	0.000
exponent for temperature, b	–0.600	0.45 ± 2.66	–0.63 ± 0.09	–0.86 ± 0.89	0.000
haze scale interval, $T_{h,1}$ (s)	4.200	4.226 ± 0.021	4.232 ± 0.020	4.38 ± 0.19	5.4 ± 2.6
haze onset interval, $T_{h,2}$ (s)	7.000	7.031 ± 0.030	7.023 ± 0.028	6.76 ± 0.28	12.7 ± 3.3
haze reference interval, $T_{H\tau 2}$ (s)	2.300	2.27 ± 0.05	2.26 ± 0.04	3.00 ± 0.69	1.4 ± 1.4
minimum observer radius, T_{min}, (s)†	46.900	70.1 ± 44.6	46.900	46.900	46.900
shadow velocity, υ (km s^{-1})	18.500	18.500	18.500	18.500	18.500
integration time, Δt (s)	0.200	0.200	0.200	0.200	0.200
Fit Information					
degrees of freedom	...	989	990	990	990
sum of squared residuals	...	3932.48	3935.21	403983	4.24743×10^7
rms residual per degree of freedom (ADU)	...	1.994	1.994	20.201	207.13

*after 1988 June 9, 10:35:50 UTC

†When fixed this number is ρ_{min}/υ = 865.69 km / 18.475911 km s^{-1}

point samples of Gaussian noise were then generated with the "ContinuousDistributions.m" package supplied with *Mathematica*™ (Wolfram 1988, version 1.2.2). These samples had rms variations of 2, 20, and 200, which represented noise that was approximately 0.1, 1.0 and 10 times that of the KAO light curve. Adding each of these noise samples to the model produced the desired synthetic light curves.

A fit to each of these light curves was obtained with standard least-squares procedures (Clifford 1973) that we implemented in *Mathematica*™. Our implementation allowed us to select any subset of the light curve for fitting and to specify for each model parameter whether it would be fixed or fit. We found it expedient to use numerical derivatives since they are easier to implement and the derivative step can be specified, allowing us to test the stability of a solution by using different step sizes. One problem with fitting data is the discontinuous derivative of our model at the top of the haze, and this can be particularly troublesome if the top of the haze corresponds to a boundary between integration bins. By limiting the size of the parameter changes to a fraction of that called for by the least-squares calculation, however, a fit could be achieved. None of the fits were weighted. A fit was considered converged when the parameters changed by no more than a few percent of their formal errors for several iterations.

The results of the fits are displayed in Table 5. For the low noise case (fit No. 1), we were able to fit for 11 free parameters. Note, however, that the formal error in the "distance of closest approach," ($T_{\rm min}$) is a large fraction of its value. The two parameters $T_{\rm min}$ and b (power law index for the temperature) both affect the second-order shape of the light curve and have a correlation greater than 0.995 for the parameter set used. Fit No. 2 of Table 5 shows the results of a fit with $T_{\rm min}$ fixed. Note the substantially lower formal error in the parameter b in fit No. 2 than in fit No. 1. Fit No. 3 of Table 5 shows the results of a fit to data of about the same noise level as the KAO data, and fit No. 4 shows a fit to data ten times noisier. For the latter fit we fixed more parameters in order to achieve convergence. Even so, with data this noisy the formal errors in the model parameters describing the haze are about equal to the values of the parameters themselves.

We draw two conclusions from our fits to synthetic data. First, we note that 22 of 28 (79%) of the fitted parameter values for the fits to the three different synthetic datasets (columns 4–6) agree with the model value of the parameter within the formal error, which is close to the average of 68% of the cases to be expected by chance. Secondly, the formal error for each fitted parameter increases approximately proportionally to the noise level in the data, which demonstrates that the linear least-squares approximation is valid for these parameter values and noise levels.

10. FITS TO THE KAO PLUTO LIGHT CURVE

We now proceed to fit our model to the stellar occultation light curve recorded with the KAO for the 1988 June 9 occultation of the star P8 (Mink & Klemola 1985; Bosh *et al.* 1986) by Pluto. As described by Elliot *et al.* (1989), these data were recorded as open-chip CCD frames, each exposed for 0.2 s with the SNAPSHOT camera (Dunham *et al.* 1985). Synthetic aperture photometry was used on the CCD frames to generate a light curve. Data over a 200 s interval used in this work were the same as that used by Elliot *et al.* (1989).

As a further test of our model fitting, we compared the results of our present model with those of Elliot *et al.* (1989), who fit the KAO data with the standard, large-planet model for the refractive flux, and then performed a first-order correction on the results for the small-planet case. To reproduce the large-planet results with the present model, we remove the small-planet corrections: (i) the r^{-2} dependence of gravity by setting $a = -2$, (ii) the temperature gradient by setting $b = 0$, (iii) the focusing effect by setting $t_{\rm em} = 10^5$ s when fitting for $t_{\rm im}$ and setting $t_{\rm im} = -10^5$ s when fitting for $t_{\rm em}$, (iv) the nonnormal limb incidence by setting $T_{\rm min} = 0$ s. The remaining differences between the two models are (i) the haze is modeled slightly differently and (ii) the present model integrates the signal over the interval containing the top of the haze and the adjacent one that corresponds to the next level deeper into the atmosphere. The results of the fits are compared in Table 6. Except for the parameters $\chi_{\tau 0}$ and $\chi_{\tau 1}$, which are defined differently from the corresponding parameters $T_{h,1}$ and $T_{h,2}$, the fitted parameters closely agree, as they should.

Next we fit the KAO data with the model-calculation and least-squares procedures described in the previous section, and the results are given in Table 7. The parameters were those of the data parameter set, summarized in Table 1. The KAO data do not have sufficiently high signal-to-noise ratio to fit for all these simultaneously. Even with the parameter b fixed at zero, the error in $T_{\rm min}$ (see fit No. 4 of Table 7) is greater than our knowledge of this quantity from the astrometric solution of Millis *et al.* (1992). Hence for all other fits this quantity was fixed. Similarly, there should be no slope in the light curve, since the sky and CCD background would have been removed, on average, by the synthetic aperture photometry. The "background" in our model would be the signal from Pluto and Charon. This would have drifted only if the extinction, instrumental gain, or seeing changed during the 200 s interval of the data. Apparently none of these effects were significant, since the fitted slope is consistent with zero. Since the background slope (s_b') and the minimum observer radius ($T_{\rm min}$ in the signal set) are known to greater accuracy by other information and their fitted values are consistent with this information, these were fixed.

A fit with a as the free parameter instead of b (fit No. 3) gives similar results to that with a fixed and b free (fit No. 2). We consider any significant value of gradient to be most likely due to a thermal, rather than a molecular weight gradient, so we chose as our solution the fit to all the data, with b a free parameter as shown as fit No. 2 in Table 7. Its fitted value, -0.61 ± 0.87, shows that Pluto's atmosphere is isothermal in this region within the precision of the model fit. The correlation coefficients between the fitted parameters are given in Table 8. Since the matrix of the correlation coefficients is symmetric, we used the upper and lower triangles of each matrix to display the coefficients of different fits. Fixed variables are represented with ellipses in these tables.

In order to check whether the atmospheric structure might be different in the regions probed by immersion and emersion, we fit these intervals of data separately. The light curve was divided into two parts at the integration interval midway between the immersion and emersion times determined from the fit to all the data. For the immersion fit, the emersion time was fixed at its value obtained from the fit to all the data, and the immersion time was fixed for the emersion fit.

Parameter values and their formal errors for the fits to the

TABLE 6. Fitted signal parameters for the KAO data for the large planet limit.

Model Parameter	Immersion, Elliot *et al.* (1989)	Immersion, Present Work	Emersion, Elliot *et al.* (1989)	Emersion, Present Work
Signal levels (per integration interval, Δt)				
Pluto	127.6 ± 1.7	127.5 ± 1.7*	125.9 ± 1.7	125.8 ± 1.7*
star	541.9 ± 2.3	542.0 ± 2.3*	542.7 ± 2.3	542.7 ± 2.3*
Isothermal atmosphere				
time of half light ($t_h = t_{im}$ or t_{em})[a]	53.79 ± 0.19	53.80 ± 0.19	139.75 ± 0.20	139.75 ± 0.20
"scale height" ($h_{obs} = T_{Hiso}$)	4.341 ± 0.114[b]	4.344 ± 0.115	4.468 ± 0.119	4.469 ± 0.119
Extinction layer				
"scale height" ($h_\tau = T_{H\tau 2}$)	3.049 ± 1.035	3.188 ± 1.066	2.729 ± 0.711	2.801 ± 0.714
top ($\chi_{\tau 0}$, $T_{h,1}$)	–0.442 ± 0.031	(4.35 ± 0.24)	–0.394 ± 0.031	(3.94 ± 0.22)
unit optical depth ($\chi_{\tau 1}$, $T_{h,2}$)	–0.676 ± 0.037	(7.10 ± 0.35)	–0.679 ± 0.038	(7.36 ± 0.36)
Fit Information†				
degrees of freedom	493	493	493	493
sum of squared residuals	183676	183735	183294	183288
rms residual per degree of freedom (ADU)	19.302	19.305	19.281	19.282

[a]seconds after 1988 June 9, 10:35:50 UTC

[b]erroneously transcribed as 0.148 in Elliot *et al.* (1989)

immersion data are shown as fit No. 6 and fit No. 7 of Table 7, and the fitted parameters for emersion are shown in the next two columns. We note that all parameter values are consistent within their formal errors for the two fits, and the value of the temperature power law, b, is consistent with zero for the fits in which it was a free parameter. The mean of the parameter values for immersion and emersion are approximately equal to their fitted value for all the data. The correlation coefficients for the immersion and emersion fits are given in Table 8.

For further analysis we shall adopt the fit to all the data that used fixed values of the background slope and scaled minimum observer radius. This is fit No. 2 of Table 7. These values and errors, along with the correlation coefficients in Table 8 are all that is needed to use the transformation equations summarized in Table 1 to calculate the atmospheric parameter set. In calculating derivatives we use numerical derivatives with a step size 0.005 times the formal error of the parameter. The KAO data are plotted as points in Fig. 6, and our adopted model is plotted as a solid line. The residuals from the model fit are also plotted in the lower part of the figure.

11. INFERENCES ABOUT PLUTO'S ATMOSPHERE

Having obtained the data parameters from fitting the KAO light curve, we now convert these to atmospheric parameters for Pluto. We have summarized all this informa-

TABLE 7. Fitted signal parameters for the KAO data.

Model Parameter	Fit #1 All Data	Fit #2 All Data b free	Fit #3 All Data a free	Fit #4 All Data s_b', T_{min} free	Fit #5 Immersion	Fit #6 Immersion b free	Fit #7 Emersion	Fit #8 Emersion b free
background level, s_b (ADU)	633.3 ± 6.8	633.1 ± 6.8	633.1 ± 6.8	632.8 ± 6.9	638.1 ± 9.7	637.6 ± 9.7	628.3 ± 9.7	628.3 ± 9.7
background slope, s_b' (ADU s^{-1})	0.0	0.0	0.0	–0.004 ± 0.011	0.0	0.0	0.0	0.0
full-scale level, s_f (ADU)	3346.3 ± 5.3	3344.2 ± 6.1	3344.2 ± 6.1	3344.2 ± 6.2	3348.7 ± 7.8	3344.9 ± 8.8	3344.4 ± 7.1	3344.3 ± 8.5
immersion half-light time, t_{im} (s*)	53.89 ± 0.15	53.94 ± 0.17	53.94 ± 0.17	53.94 ± 0.17	53.75 ± 0.20	53.82 ± 0.23	53.937729	53.937729
emersion half-light time, t_{em} (s*)	139.92 ± 0.15	139.88 ± 0.17	139.88 ± 0.17	139.87 ± 0.17	139.8769	139.8769	139.77 ± 0.21	139.78 ± 0.22
refraction scale interval, T_{Hiso} (s)	4.61 ± 0.09	4.71 ± 0.18	4.71 ± 0.19	4.71 ± 0.17	4.54 ± 0.13	4.70 ± 0.23	4.68 ± 0.13	4.68 ± 0.27
exponent for molecular weight, a	0.0	0.0	–0.66 ± 0.86	0.0	0.0	0.0	0.0	0.0
exponent for temperature, b	0.0	–0.61 ± 0.87	0.0	0.0	0.0	–1.02 ± 1.16	0.0	–0.01 ± 1.39
haze scale interval, $T_{h,1}$ (s)	4.16 ± 0.17	4.11 ± 0.19	3.95 ± 0.33	4.11 ± 0.19	4.39 ± 0.24	4.30 ± 0.27	3.98 ± 0.21	3.98 ± 0.19
haze onset interval, $T_{h,2}$ (s)	7.10 ± 0.25	7.01 ± 0.28	6.86 ± 0.40	7.02 ± 0.28	6.99 ± 0.34	6.85 ± 0.38	7.19 ± 0.36	7.19 ± 0.41
haze reference interval, $T_{H\tau 2}$ (s)	2.27 ± 0.41	2.34 ± 0.44	2.35 ± 0.44	2.36 ± 0.45	2.39 ± 0.71	2.52 ± 0.76	2.22 ± 0.51	2.22 ± 0.54
minimum observer radius, T_{min}, (s)†	46.855064	46.855064	46.855064	61.72 ± 25.10	46.855064	46.855064	46.855064	46.855064
Fit Information								
degrees of freedom	992	991	991	990	478	477	508	507
sum of squared residuals	374043	373875	373877	373814	180602	180338	191805	191804
rms residual per degree of freedom (ADU)	19.418	19.424	19.424	19.432	19.438	19.444	19.431	19.450

*after 1988 June 9, 10:35:50 UTC

†When fixed this number is ρ_{min}/v = 865.69 km / 18.475911 km s^{-1}

TABLE 8. Correlation coefficients for fits to the KAO data.

(a) All Data, Fits #1 and #2 of Table 7

Model Parameter	s_b	s_f	t_{im}	t_{em}	T_{Hiso}	b	$T_{h,1}$	$T_{h,2}$	$T_{H\tau 2}$
s_b	**1.00**	–0.03	–0.30	0.30	–0.16	...	0.22	–0.02	–0.49
s_f	0.01	**1.00**	–0.10	0.10	0.34	...	0.07	0.00	0.04
t_{im}	–0.30	–0.28	**1.00**	–0.81	0.64	...	–0.85	–0.66	0.28
t_{em}	0.30	0.28	–0.84	**1.00**	–0.64	...	0.85	0.66	–0.28
T_{Hiso}	–0.13	–0.29	0.65	–0.65	**1.00**	...	–0.62	–0.56	0.22
b	0.05	0.52	–0.38	0.38	–0.83	**1.00**	...	...	...
$T_{h,1}$	0.23	0.27	–0.88	0.89	-0.65	0.39	**1.00**	0.56	–0.10
$T_{h,2}$	0.02	0.25	–0.72	0.73	–0.66	0.46	0.65	**1.00**	–0.38
$T_{H\tau 2}$	–0.49	–0.08	0.34	–0.34	0.31	–0.23	–0.19	–0.44	**1.00**

(b) All Data, Fits #3 and #4 of Table 7

Model Parameter	s_b	s_b'	s_f	t_{im}	t_{em}	T_{Hiso}	a	$T_{h,1}$	$T_{h,2}$	$T_{H\tau 2}$	T_{min}
s_b	**1.00**	...	0.01	–0.30	0.30	–0.13	0.05	0.16	0.04	–0.49	...
s_b'	0.02	**1.00**	...	...	...	...	...	...	...	...	...
s_f	0.02	–0.08	**1.00**	–0.28	0.28	–0.30	0.52	0.47	0.40	–0.09	...
t_{im}	–0.30	0.12	–0.31	**1.00**	–0.85	0.64	–0.38	–0.75	–0.69	0.34	...
t_{em}	0.31	0.06	0.29	–0.84	**1.00**	–0.64	0.38	0.75	0.69	–0.34	...
T_{Hiso}	–0.16	0.03	–0.29	0.67	–0.67	**1.00**	–0.85	–0.91	–0.86	0.32	...
a	...	...	...	...	...	...	**1.00**	0.84	0.77	–0.23	...
$T_{h,1}$	0.24	–0.03	0.28	–0.88	0.88	–0.67	...	**1.00**	0.86	–0.26	...
$T_{h,2}$	0.02	–0.03	0.24	–0.73	0.73	–0.65	...	0.65	**1.00**	–0.42	...
$T_{H\tau 2}$	–0.50	0.01	–0.10	0.35	–0.35	–0.20	...	–0.20	–0.44	**1.00**	...
T_{min}	–0.08	0.06	–0.53	0.41	–0.40	–0.42	...	–0.42	–0.43	0.25	**1.00**

(c) Immersion Data, Fits #5 and #6 of Table 7

Model Parameter	s_b	s_f	t_{im}	T_{Hiso}	b	$T_{h,1}$	$T_{h,2}$	$T_{H\tau 2}$
s_b	**1.00**	–0.03	–0.31	–0.16	...	0.20	0.01	–0.50
s_f	0.00	**1.00**	–0.11	0.35	...	0.07	0.01	0.04
t_{im}	–0.31	–0.29	**1.00**	0.65	...	–0.88	–0.69	0.27
T_{Hiso}	–0.14	–0.26	0.68	**1.00**	...	–0.60	–0.54	0.19
b	0.05	0.51	–0.38	–0.81	**1.00**	...	...	...
$T_{h,1}$	0.21	0.26	–0.91	–0.66	0.39	**1.00**	0.53	–0.04
$T_{h,2}$	0.05	0.24	–0.76	–0.65	0.44	0.64	**1.00**	–0.40
$T_{H\tau 2}$	–0.51	–0.07	0.32	0.27	–0.20	–0.13	–0.45	**1.00**

(d) Emersion Data, Fits #7 and #8 of Table 7

Model Parameter	s_b	s_f	t_{em}	T_{Hiso}	b	$T_{h,1}$	$T_{h,2}$	$T_{H\tau 2}$
s_b	**1.00**	–0.03	0.33	–0.17	...	0.29	–0.04	–0.49
s_f	0.01	**1.00**	0.09	0.34	...	0.08	–0.01	0.05
t_{em}	0.34	0.29	**1.00**	–0.67	...	0.97	0.70	–0.36
T_{Hiso}	–0.14	–0.34	–0.65	**1.00**	...	–0.66	–0.57	0.29
b	0.07	0.54	0.40	–0.87	**1.00**	...	...	...
$T_{h,1}$	0.32	0.29	0.99	–0.65	0.41	**1.00**	0.66	–0.30
$T_{h,2}$	0.01	0.25	0.76	–0.66	0.47	0.75	**1.00**	–0.38
$T_{H\tau 2}$	–0.49	–0.13	–0.49	0.42	–0.31	–0.45	–0.49	**1.00**

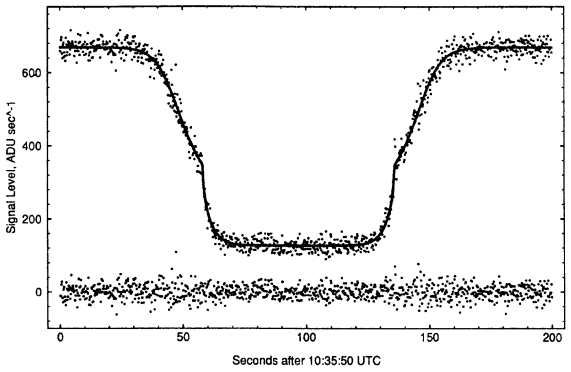

FIG. 6. Stellar-occultation data and model. The stellar-occultation light curve observed with the KAO (Elliot *et al.* 1989) has been plotted as points and the best-fitting model as a line. The residuals from the model fit are the points in the lower part of the the figure. The few points with the largest residuals occur where the light curve has the largest slope, and they represent unmodeled density variations in Pluto's atmosphere.

tion about Pluto's atmosphere in Table 9, in which the parameters have been divided into five groups: (i) "physical," which includes Pluto's mass and physical properties of gases; (ii) "specific to the KAO light curve," which includes the signal levels of the KAO light curve and geometry of the occultation; (iii) "clear atmosphere," which includes parameters that apply to Pluto's atmosphere corresponding to levels above the break in the light curve; (iv) "haze, no steep thermal gradient," which includes parameters that apply to the haze model for Pluto's atmosphere (Elliot *et al.* 1989 and this work); (v) "steep thermal gradient, no haze," which includes parameters that apply to Pluto's atmosphere if the thermal gradient model for the lower atmosphere is correct (Eshleman 1989; Hubbard *et al.* 1990).

In addition to the uncertainty between the haze and thermal gradient models for Pluto's lower atmosphere, another major uncertainty is the composition of the atmosphere. Accordingly, the second column of Table 9 gives values of quantities that are independent of an assumed atmospheric composition, and each of the following four columns gives parameters for an assumed composition. The first of these is 100% CH_4, which could be the limiting case if radiative cooling of the atmosphere is not the 7.8 μm band of CH_4, but through a band of longer wavelength—such as the 13.7 μm band of C_2H_2, which dominates the radiative cooling in Titan's atmosphere (Lellouch *et al.* 1990). The next three columns give limiting cases that would apply if the atmosphere were in radiative equilibrium dominated by the 7.8 μm band of CH_4 (Yelle & Lunine 1989; Hubbard *et al.* 1990). These are cases that would give a mean molecular weight near 28: 100% N_2, 100% CO, and 50% CH_4-50% Ar.

Now we describe the entries in Table 9 in more detail, working our way down from the top. Determination of the Pluto–Charon mass ratio by measuring the "wobble" of the system center of light is in progress, but the result is not yet available (Wasserman *et al.* 1988). Beletic *et al.* (1989) determined the mass of the Pluto–Charon system to be $(1.35 \pm 0.07) \times 10^8\ \mathcal{M}_\odot{}^{-1}$ by measuring the semimajor axis of the Pluto–Charon orbit and combining this with the well-determined orbital period (Tholen & Buie 1990). Using this value for the system mass, one could infer a mass for Pluto alone by calculating the relative volumes of Pluto and Charon from the mutual event radii (Tholen & Buie 1990) and adding some additional uncertainty corresponding to the unknown relative densities for the two bodies. However, we cannot accept the radius of Pluto and its error determined from the mutual events as the surface radius, since this radius refers to the visible disk of Pluto, which may or may not be the surface. Furthermore, the mutual-event radius for Pluto's visible disk is at odds with with the visible-disk radius determined by combining stellar occultation chords from the 1988 June 9 event (Millis *et al.* 1992).

We see two likely sources for the radius inconsistency, both connected with the mutual-event radius: (i) unmodeled limb darkening of Pluto that would cause the mutual event radius to be underestimated, and (ii) an unidentified systematic error (or underestimate of the error) in the semimajor axis of the system, which would propagate proportionally into the radius. Hence, for our present purpose, we use Beletic *et al.*'s (1989) system mass, but we increase its error from $0.075 \times 10^8\ \mathcal{M}_\odot{}^{-1}$ to $0.226 \times 10^8\ \mathcal{M}_\odot{}^{-1}$, a value set by requiring that the 1σ error on the mutual event radius for Pluto should include the stellar occultation radius for the visible disk of Pluto. This corresponds to a semimajor-axis error of $\pm$ 1100 km (cf. 19 640 $\pm$ 320 km from Beletic *et al.*). Next, we derive an expression for Pluto's mass, in terms of the Pluto–Charon semimajor axis, and Charon's mass, calculated under the assumption that its density is 2.0 ± 1.0 g cm^{-3} and its radius is 593 ± 13 km (Tholen & Buie 1990), with additional uncertainty from semimajor-axis error. The resulting Pluto mass is $\mathcal{M}_p = (1.30 \pm 0.24) \times 10^{25}$ g, as has been entered in Table 9.

The refractivities of CH_4, N_2, CO, and Ar at standard temperature and pressure (ν_{STP}) were calculated by integrating the refractivity of each gas over the quantum efficiency function for our CCD chip (Dunham *et al.* 1985) and the photon emission function for a black body at 4900 K, which would have the same *BVR* colors as the occulted star, P8 (Bosh *et al.* 1986).

In the next group of parameters, "specific to the KAO light curve," we find the background level, star level, and midtime through conversion of the fitted data parameter set given in the second column of Table 7 to the atmospheric parameter set. The resulting correlation coefficients for the new parameters are given in Table 10. In this conversion we have chosen a fixed reference radius of 1250 km, the same as that used by Millis *et al.* (1992). Recall that the reference radius has no error bar, since this is a fixed parameter that is selected for convenience. All parameters in Table 9 belonging to the atmospheric set have been flagged with an asterisk (*). Some of these are used to derive other parameters describing the atmosphere, since correlation coefficients are available for this set (Table 10) that allow the calculation of formal errors for any derived parameter.

Quantities pertinent to the occultation geometry, D and v and ρ_{min}, have been provided by Millis *et al.* (1992). As errors in D and v are difficult to estimate, yet certainly far too small to significantly affect the error on quantities derived from them, we have not attempted to enter their errors in Table 9. As we have seen in our fitting experiments, ρ_{min} is poorly determined by the shape of the light curve, so we use the value of 865.69 km, determined by a joint fit to all Pluto occultation data for this event (Millis *et al.* 1992). The error on this value is composed of two parts: (i) the error in deter-

TABLE 9. The structure of Pluto's atmosphere.

Parameters	Values That Are Independent of Composition	Assumption for Composition			
		100% CH_4	100% N_2	100% CO	50% CH_4 50% Ar
Physical					
Pluto mass, M_p (g)	$(1.30 \pm 0.24) \times 10^{25}$				
molecular weight, μ_0 (amu)		16.04	28.01	28.01	28.00
refractivity, ν_{STP} (10^{-4})†		4.401	2.980	3.364	3.614
Specific To the KAO Light Curve					
background level, s_b (ADU s^{-1})	633.1 ± 6.8*				
background slope, s_b' (ADU s^{-2})	0.0				
star level, s_* (ADU s^{-1})	2711.2 ± 9.1*				
midtime, t_{mid} (s)	96.907 ± 0.046*				
planet-observer distance, D (km)	4.323×10^9§				
minimum observer radius, ρ_{min} (km)	865.69 ± 15.00§				
shadow velocity, v (km s^{-1})	18.4759§				
Clear Atmosphere					
reference radius, r_0 (km)	1250				
refractivity, ν_0 (10^{-9})	0.97 ± 0.17*				
energy ratio, λ_{g0}	22.4 ± 1.8*				
power index for temperature, b	−0.61 ± 0.87*				
gravity, g_0 (cm sec^{-2})	56 ± 10				
pressure scale height, H_{p0} (km)	55.7 ± 4.5				
temperature, T_0 (K)	$(3.72 \pm 0.75)\ \mu_0$	60 ± 12	104 ± 21	104 ± 21	104 ± 21
temperature gradient, $(dT/dr)_0$ (K km^{-1})	$(-4.9 \pm 7.0) \times 10^{-4} T_0$	−0.029 ±0.040	−0.051 ±0.070	−0.051±0.070	−0.051±0.070
number density, n_0 (10^{14} cm^{-3})	$(2.61 \pm 0.46) \times 10^{-4}/\nu_{STP}$	0.59 ± 0.11	0.88 ± 0.16	0.78 ± 0.14	0.72 ± 0.13
pressure, p_0 (μbar)	$(1.38 \pm 0.38) \times 10^{-5}\ \mu_0/\nu_{STP}$	0.49 ± 0.14	1.26 ± 0.35	1.12 ± 0.31	1.04 ± 0.29
column height, ξ_0 (cm-A)		13.4 ± 2.8	19.8 ± 4.1	17.5 ± 3.7	16.3 ± 3.4
number density, n_1 (10^{14} cm^{-3})		1.102 ± 0.041	1.627 ± 0.060	1.442 ± 0.053	1.342 ± 0.050
pressure, p_1 (μbar)		0.92 ± 0.19	2.38 ± 0.49	2.10 ± 0.44	1.96 ± 0.41
column height, ξ_1 (cm-A)		23.9 ± 2.3	35.3 ± 3.4	31.3 ± 3.0	29.1 ± 2.8
Haze, No Steep Thermal Gradient					
top of haze, r_1 (km)	1215 ± 11*				
haze scale height, $H_{\tau 1}$ (km)	29.8 ± 5.6*				
linear absorption coefficient, $\kappa_{\tau 1}$ (cm^{-1})	$(2.22 \pm 0.18) \times 10^{-8}$*				
surface radius (km)	≤ 1181				
vertical thickness of haze (km)	≥ 34				
vertical optical depth, τ_V	≥ 0.145				
surface number density, n_s (10^{14} cm^{-3})		≥ 2.1	≥ 3.1	≥ 2.7	≥ 2.5
surface pressure, p_s (μbar)		≥ 1.8	≥ 4.5	≥ 4.1	≥ 3.8
surface column height, ξ_s (cm-A)		≥ 43	≥ 64	≥ 57	≥ 53
surface temperature, T_s (K)	34-58¶	>48.8	>35.7	>39.5	>49.0
bulk density (g cm^{-3})	> 1.88				
Steep Thermal Gradient, No Haze					
surface radius, r_s (km)	1206 ± 11				
surface number density, n_s (10^{14} cm^{-3})		1.70 ± 0.38	6.77 ± 1.69	5.31 ± 1.30	3.86 ± 0.91
surface pressure, p_s (μbar)		1.12 ± 0.26	3.25 ± 0.84	2.83 ± 0.71	2.54 ± 0.62
surface column height, ξ_s (cm-A)		28.5 ± 3.3	47.1 ± 7.9	41.0 ± 6.5	37.0 ± 5.3
surface temperature, T_s (K)	34-58¶	48.04 ± 0.45	35.25 ± 0.37	39.02 ± 0.38	48.29 ± 0.48
bulk density (g cm^{-3})	1.77 ± 0.33				

† *e. g.* multiply entry by 10^{-4}
* one of the 9 "atmospheric" parameters obtained from conversion of the "data" parameters
§ after Mills *et al.* (1992)
¶ range of published values; see text.

mining the center of the shadow, and (ii) the error in the KAO position. The error in the KAO position is about 15 km (unnecessarily large, due to inadequate navigational equipment). Since the error in the shadow center is much less than this (Millis *et al.* 1992), we adopt an error of 15 km for ρ_{min}, which has been entered in Table 9.

Some of the parameters that describe the "clear atmosphere"—refractivity, energy ratio, and power index for the temperature—are obtained directly from the conversion from the data parameters. For the KAO light curve, the model is most sensitive to a thermal gradient at a radius of 1427 km from the center of Pluto, within a range of 153 km (FWHM). The other parameters in this group were calculated from parameters higher in Table 9 with Eqs. (6.11)–(6.21). Errors for these parameters were calculated by propagating errors from more fundamental parameters, accounting for correlations of these parameters (Table 10). Since the temperature-to-molecular-weight ratio is relatively well determined, the temperature of this region of the atmosphere could be as low as 60 ± 12 K in the limit of a pure

TABLE 10. Correlation coefficients for atmospheric parameters.

Model Parameter	s_b	s_*	t_{mid}	ν_0	λ_{g0}	b	r_1	κ_1	$H\tau 1$
s_b	**1.00**	–0.80	0.00	0.01	0.10	...	0.02	–0.13	–0.49
s^*	–0.74	**1.00**	0.00	0.08	–0.19	...	0.02	0.13	0.41
t_{mid}	0.00	0.00	**1.00**	0.00	0.00	...	0.00	0.01	0.00
ν_0	0.03	0.17	0.00	**1.00**	0.65	...	0.98	0.03	–0.03
λ_{g0}	–0.01	–0.36	0.00	–0.15	**1.00**	...	0.77	–0.06	–0.18
b	0.05	0.31	0.00	0.35	–0.94	**1.00**	...	...	...
r_1	0.03	0.05	0.00	0.95	0.14	0.10	**1.00**	0.00	–0.07
κ_1	–0.13	0.07	0.01	–0.02	0.13	–0.16	–0.02	**1.00**	0.79
$H\tau 1$	–0.49	0.31	0.00	–0.11	0.15	–0.23	–0.09	0.79	**1.00**

methane atmosphere. This magnitude and error of this result differs from that of our previous analysis (Elliot *et al.* 1989, 67 ± 6 K for a pure methane atmosphere). The difference in the value arises from approximations made in the earlier work. The dominant source of error in the temperature comes from the mass error. Hence the present error in the atmospheric temperature is larger in this work because we used what we feel is a more realistic error for Pluto's mass, which is twice that of our previous work.

The next set of parameters, "haze, no steep thermal gradient," are valid if the haze model described in this paper correctly describes the lower part of Pluto's atmosphere. The first three of these parameters—top of the haze, haze scale height, and linear absorption coefficient—are obtained directly from the conversion of parameters from the data parameter set. For this model the surface radius is not known—only that it must lie below a level corresponding to that where we can still detect light from the occultation curve. From the limit that the surface radius must be less than 1181 km, we derive a lower limit on the vertical optical depth of the haze of 0.145, a value not great enough to obscure the observed repeatable variations in the Pluto–Charon rotational light curve. Also from the limit on the surface radius, we derive limits on the surface number density and pressure for our assumptions for the atmospheric composition. We can also derive lower limits on the surface temperature if we assume that the atmosphere is in vapor-ice equilibrium (Brown & Ziegler 1980). For the CH_4-Ar mixture, we assumed that the CH_4 was in vapor-ice equilibrium, and that the Ar fraction is limited by an equilibrium between unspecified resupply and escape processes. These lower limits on surface temperatures can be compared with the range of surface temperatures for Pluto between 31 and 59 K that have been derived from *IRAS* and mm observations of Pluto–Charon, analyzed under various assumptions about the thermal properties of the surfaces of Pluto and Charon (Sykes *et al.* 1987; Aumann & Walker 1987; Tedesco *et al.* 1987; Altenhoff *et al.* 1988).

If the haze model is not correct and a steep thermal gradient is causing the observed break in the KAO occultation curve (Eshleman 1989; Hubbard *et al.* 1990), then the parameters listed in "steep thermal gradient, no haze" apply to Pluto. To derive these parameters we have assumed that the surface radius lies 9 ± 3 km below the level corresponding to the break in the light curve, a value found from the theoretical thermal profiles for a clear Plutonian atmosphere (Hubbard *et al.* 1990). This gives us a surface radius of 1206 ± 11 km. We found thermal and pressure profiles for this layer by matching the temperature and pressure at r_1 and assuming the gas is in vapor-ice equilibrium at the surface. For the CH_4-Ar mixture, we assume the CH_4 fraction is in vapor-ice equilibrium, as we did for the haze model.

In Fig. 7 we have summarized the main features of Pluto's atmosphere (as given in Table 9) and the relation of the atmosphere to the surface, where the radius is plotted as the ordinate and temperature along the abscissa. The left panel illustrates the structure for the thermal-gradient model and the right panel shows the structure for the haze model. For each of these cases we have the further uncertainty of the atmospheric composition. We know that the upper part of the atmosphere contains some methane, but the range of possible methane fractions is large. The temperature could be greater than 100 K, if the model of Yelle & Lunine (1989) is correct and the main cooling process is radiation through the 7.8 μm band of CH_4. However, if the primary cooling is through other bands at longer wavelengths, then the temperature would be less. Some type of thermostatic action is likely at work in this region, since our results indicate that the atmosphere is isothermal here.

Below this clear region of the atmosphere, whose boundary is delineated by the break in the occultation light curve, we do not know the atmospheric structure. This region may be the onset of a sharp thermal gradient, in which case the surface of Pluto would lie only a few kilometers below. This boundary could also mark the onset of a haze layer, as we have modeled here. We infer that the haze cannot be optically thick, since Pluto's light curve could not have such a large amplitude and be in phase with the orbital period of Charon (which is most likely tidally locked to the rotation of Pluto). However, if the effects of haze are dominating the light-curve structure, we have no lower bound on Pluto's surface radius, since we do not know whether the haze is layered or uniformly mixed with the atmosphere. We might set a limit on the surface radius by arguing that Pluto's density would likely not exceed a certain value—say 3.0 g cm^{-3}. Although this approach can be used to set a limit on the surface radius, it is of marginal value, since the point of finding the surface radius is to learn the density of Pluto.

12. CONCLUSIONS

The presence of a thermal gradient in the atmosphere of an occulting planet can significantly affect the shape of a stellar-occultation light curve. Furthermore, the value of the

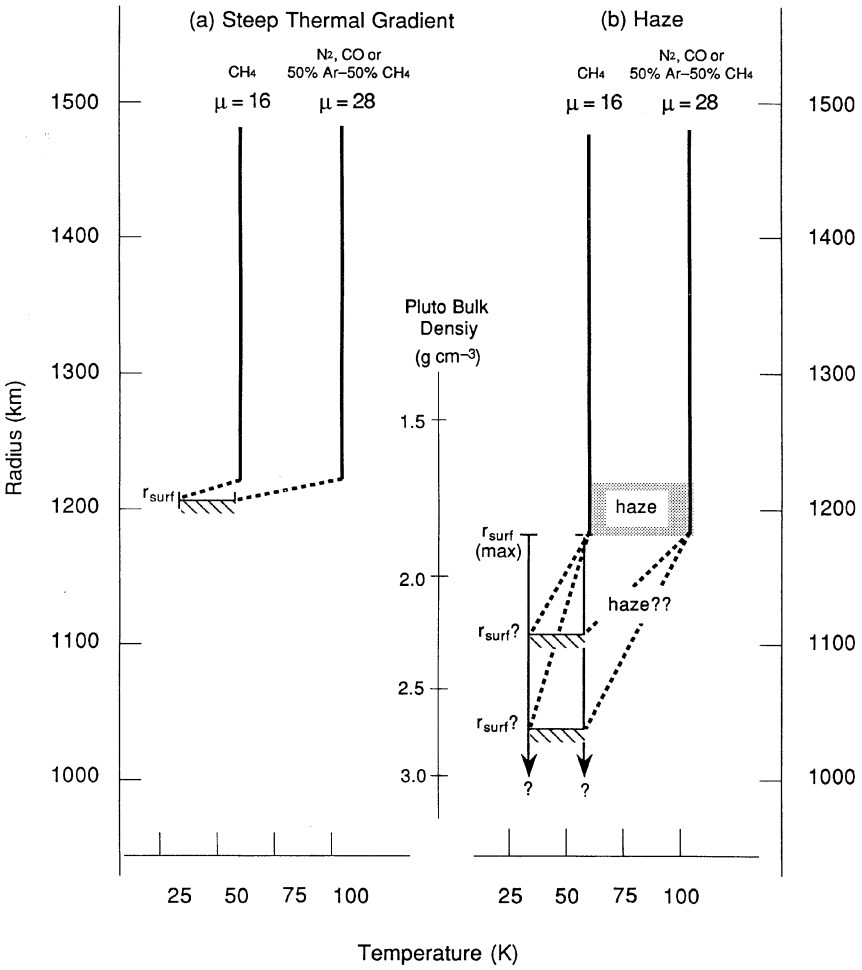

FIG. 7. Possible atmospheric structures of Pluto. Temperature profiles in this figure illustrate the two main uncertainties we presently have about Pluto's atmosphere: (i) its composition, and (ii) the existence of a haze layer. Each of the two panels corresponds to a different explanation for the drop in light curve: (a) a steep thermal gradient just above the surface, and (b) a haze layer. Solid lines indicate the temperature in a near-isothermal region. The haze model assumes a near-isothermal atmosphere until 1181 km, where the star is last detectable in the light curve (the surface can be anywhere below this). Dashed lines indicate possible thermal profiles between the upper region and the surface. Values of the surface temperature inferred from *IRAS* and mm observations are indicated by the lower positions of the dashed lines. In the steep thermal gradient case, inversions of the light curve predict a surface ~9 km lower than the onset of the gradient (Eshleman 1989; Hubbard *et al.* 1990). The haze can continue down to the surface or be a detached layer, so limits on the vertical optical depth do not constrain the surface radius. Therefore the two models predict different surface radii and corresponding bulk densities for Pluto. For convenience, the bulk density for Pluto corresponding to a surface radius on the outer scales can be read from the scale between the two panels.

gradient can be found by fitting a model light curve to data of good signal-to-noise ratio. Using our method to analyze the KAO Pluto occultation data, we find that the upper part of Pluto's atmosphere probed by the stellar occultation is isothermal: $dT/dr = -0.029 \pm 0.040$ K km^{-1} for the limiting case of pure CH_4 and -0.051 ± 0.070 K km^{-1} for the limiting case of pure N_2. This result is consistent with the isothermal prediction of Yelle & Lunine's (1989) methane-thermostat model. However, Pluto's atmosphere could be isothermal in this region at a temperature less than the 106 K calculated by their model, if the thermostatic action is controlled by a molecular band that has a wavelength longer than the 7.8 μm band of CH_4. Hence we still cannot constrain the CH_4 fraction in the atmosphere, and we cannot determine from present observations the identity and amounts of other gases.

Another unknown in the region of Pluto's atmosphere probed by the occultation data is whether a haze or thermal gradient dominates the structure of the lower part of Pluto's atmosphere. If the thermal-gradient model is correct, then Pluto's surface radius is 1206 ± 11 km, and its bulk density is 1.77 ± 0.33 g cm^{-3}. On the other hand, if the haze model is correct, we can say only that Pluto's surface radius is less than 1181 km and its bulk density is greater than 1.88 g cm^{-3}.

Further progress toward a first-order model of Pluto's atmosphere requires answers to these two questions: (i) exactly what gases are present, and in what proportions?, and (ii) does the sharp break in the slope of the KAO stellar occultation curve delineate the top of an extinction layer or the onset of a large thermal gradient, ~10 K km^{-1}? The answer to the second question is also a prerequisite to pinning down the density of Pluto to the accuracy we would like for comparison with formation models for Pluto and Charon.

A direct observational test of the haze versus thermal gradient question would be the observation of a future stellar occultation simultaneously at infrared and visible wavelengths: micron-size haze particles would have significantly lower optical depth in the near infrared than at visible wavelengths. An opportunity for carrying out such an observation occurs on 1992 May 21 (UT), when Pluto will likely occult a star with $R = 13.0$, visible from the western hemisphere (Mink *et al.* 1991; Dunham *et al.* 1991).

We are grateful to L. H. Wasserman for comparing his model calculations and least-squares-fit results with ours, and to R. L. Millis *et al.* for supplying the value of the KAO minimum observer radius and shadow velocity in advance of publication. This work was supported, in part, by NASA Grant No. NAGW-1494 and NSF Grant No. AST-8906011.

APPENDIX: POWER SERIES

In this appendix we present the power series for use with the equations for the refraction angle, $\theta(r)$ [Eq. (4.6)], the derivative of the refraction angle, $d\theta/dr$ [Eq. (4.9)], and the optical depth along the path of the light ray, $\tau_{\rm obs}(r)$ [Eq. (4.19)].

The series required by the refraction angle—denoted by $A(\delta,a,b)$—is a function of the parameter δ [Eq. (4.2)], the exponent for molecular weight variation, a [Eq. (3.1)] and the exponent for temperature variation, b [Eq. (3.3)]. As discussed in Sec. 4, $\delta\rightarrow 0$ in the large planet limit, and if there are no temperature or molecular weight gradients in the atmosphere, then $a=b=0$.

We obtained the series $A(\delta,a,b)$ by performing the integral in Eq. (4.5). The integrand is expanded to 4th order in δ, after which it contains a polynomial in y, the variable of integration, and δ, the expansion parameter of our series. By expanding the integrand in δ rather than y, we guarantee that the series is complete in y for a given order of δ. Each term of δ has as a coefficient a power series in a and b. We evaluate the resulting integrals, term by term. The definite integrals that arise in this expansion are of the following form (Dwight 1961, by manipulation of Sec. 860.17):

$$\int_{-\infty}^{\infty} y^n e^{-y^2} dx = \begin{cases} \Gamma\left(\dfrac{n+1}{2}\right) = \dfrac{(n-1)!\sqrt{\pi}}{2^n (n/2)!}, & n \text{ even} \\ 0, & n \text{ odd} \end{cases} . \tag{A1}$$

The resulting series, calculated with *Mathematica*™ (Wolfram 1988), is

$$\begin{aligned} A(\delta,a,b) = 1 &+ \left(-\frac{3+a}{8}+\frac{3b}{8}\right)\delta + \left(-\frac{15+26a+7a^2}{128}+\frac{7+5a}{64}b+\frac{b^2}{128}\right)\delta^2 \\ &+ \left(-\frac{105+425a+355a^2+75a^3}{1024}+\frac{27+50a+35a^2}{1024}b+\frac{69+55a}{1024}b^2+\frac{9}{1024}b^3\right)\delta^3 \\ &+ \left(-\frac{4725+35196a+57134a^2+31836a^3+5509a^4}{32768}-\frac{1059+4907a+3857a^2+609a^3}{8192}b \right. \\ &\left. + \frac{2353+4326a+2233a^2}{16384}b^2+\frac{3764+3164a}{8192}b^3+\frac{491}{32768}b^4\right)\delta^4+\cdots \end{aligned} \tag{A2}$$

The series for the derivative of the refraction angle, $B(\delta,a,b)$, is found from Eq. (4.6) by taking the derivative of $\theta(r)$:

$$\frac{d\theta(r)}{dr} = -\sqrt{2\pi\lambda_g(r)}\,\nu(r)\left[\left(\frac{1}{\sqrt{\lambda_g(r)}}\frac{d\sqrt{\lambda_g(r)}}{dr}+\frac{1}{\nu(r)}\frac{d\nu(r)}{dr}\right)A(\delta,a,b)+\frac{dA(\delta,a,b)}{dr}\right]. \tag{A3}$$

We evaluate the derivatives, and factor $\lambda_g(r)/r$ out of the brackets. Recall that $d\lambda_g(r)/dr = -\lambda_g(r)(1+a+b)/r$ [from Eq. (3.9)], $(1/\nu)d\nu/dr = -1/H_n = -(\lambda_g+b)/r$, and $d\delta/dr = \delta(1+a+b)/r$. With these substitutions, the derivative becomes

$$\frac{d\theta(r)}{dr} = \sqrt{2\pi\lambda_g^3(r)}\,\frac{\nu(r)}{r}\left[\left(\frac{(1+a+b)\delta}{2}+1+b\delta\right)A(\delta,a,b)-\frac{1+a+b}{2}\delta^2\frac{dA(\delta,a,b)}{d\delta}\right]. \tag{A4}$$

By comparison with Eq. (4.9), we see that $B(\delta,a,b)$, the series needed for $d\theta/dr$, can be expressed in terms of the series for $\theta(r)$:

$$B(\delta,a,b) = \left(1+\frac{1+a+3b}{2}\delta\right)A(\delta,a,b)-\frac{1+a+b}{2}\delta^2\frac{dA(\delta,a,b)}{d\delta}. \tag{A5}$$

Substituting $A(\delta,a,b)$ into the previous expression, we find

$$\begin{aligned} B(\delta,a,b) = 1 &+ \left(\frac{1+3a}{8}+\frac{15}{8}b\right)\delta + \left(\frac{9+6a+a^2}{128}-\frac{17+11a}{64}b+\frac{25b^2}{128}\right)\delta^2 \\ &+ \left(\frac{75+67a+41a^2+9a^3}{1024}-\frac{81+134a+57a^2}{1024}b+\frac{1+3a}{1024}b^2+\frac{5b^3}{1024}\right)\delta^3 \\ &+ \left(\frac{3675+7204a+5266a^2+2564a^3+491a^4}{32768}-\frac{339+1347a+1297a^2+409a^3}{8192}b \right. \\ &\left. - \frac{10555+1834a+807a^2}{16384}b^2-\frac{67+49a}{8192}b^3+\frac{59}{32768}b^4\right)\delta^4+\cdots \end{aligned} \tag{A6}$$

For the series required by the line-of-sight optical depth, we follow the procedure outlined in Sec. 4. The expansion parameter is $\delta_\tau \equiv H_{\tau 1} r/r_1^2$, and the resulting power series is

$$C(\delta_\tau) = 1+\frac{9}{8}\delta_\tau+\frac{345}{128}\delta_\tau^2+\frac{9555}{1024}\delta_\tau^3+\frac{1371195}{32768}\delta_\tau^4+\cdots \tag{A7}$$

REFERENCES

tenhoff, W. J., Chini, R., Hein, H., Kreysa, E., Mezger, P. G., Salter, C., & Schraml, J. B. 1988, A&A, 190, L15
ımann, H. H., & Walker, R. G. 1987, AJ, 94, 1088
.um, W. A., & Code, A. D. 1953, AJ, 58, 108
letic, J. W., Goody, R. M., & Tholen, D. J. 1989, Icarus, 79, 38
ısh, A. S., Elliot, J. L., Kruse, S. E., Baron, R. L., Dunham, E. W., & French, L. M. 1986, Icarus, 66, 556
own, Jr., G. N., & Ziegler, W. T. 1980, Adv. Cryog. Eng., 25, 662
ifford, A. A. 1973, Multivariate Error Analysis (Applied Science, London)
ınham, E. W., Baron, R. L., Elliot, J. L., Vallerga, J. V., Doty, J. P., & Ricker, G. R. 1985, PASP, 97, 1196
ınham, E. W., McDonald, S. W., & Elliot, J. L. 1991, AJ, 102, 1464
ıight, H. B. 1961, Tables of Integrals and other Mathematical Data (Macmillan, New York)
liot, J. L., Dunham, E. W., Bosh, A. S., Slivan, S. M., Young, L. A., Wasserman, L. H., & Millis, R. L. 1989, Icarus, 77, 148
liot, J. L., French, R. G., Dunham, E., Gierasch, P. J., Veverka, J., Church, C., & Sagan, C. 1977, ApJ, 217, 661
liot, J. L., French, R. G., Meech, K. J., & Elias, J. H. 1984, AJ, 89, 1587
liot, J. L., Rages, K., & Veverka, J. 1976, ApJ, 207, 994
liot, J. L., & Veverka, J. 1976, Icarus, 27, 359
hleman, V. R. 1989, Icarus, 80, 439
French, R. G., Elliot, J. L., & Gierasch, P. J. 1978, Icarus, 33, 186
Goldsmith, D. W. 1963, Icarus, 2, 341
Hubbard, W. B., Hunten, D. M., Dieters, S. W., Hill, K. M., & Watson, R. D. 1988, Nature, 336, 452
Hubbard, W. B., Yelle, R. V., & Lunine, J. I. 1990, Icarus, 84, 1
Lellouch, E., Hunten, D. M., Kockarts, G., & Coustenis, A. 1990, Icarus, 83, 308
Maeder, R. E. 1990, Programming in Mathematica (Addison–Wesley, Reading)
Millis, R. L., *et al.* 1992, in preparation
Mink, D. J., & Klemola, A. 1985, AJ, 90, 1894
Mink, D. J., Klemola, A. R., & Buie, M. W. 1991, AJ, 101, 2255
Sykes, M. V., Cutri, R. M., Lebofsky, L. A., & Binzel, R. P. 1987, Sci, 237, 1336
Tedesco, E. F., Veeder, Jr., G. J., Dunbar, R. S., & Lebofsky, L. A. 1987, Nature, 327, 127
Tholen, D. J., & Buie, M. W. 1990, BAAS, 22, 1129
Wasserman, L. H., Millis, R. L., Franz, O. G., Klemola, A. R., & Dahn, C. C. 1988, BAAS, 20, 806
Wasserman, L. H., & Veverka, J. 1973, Icarus, 20, 322
Wolfram, S. 1988, Mathematica (Addison–Wesley, Reading)
Yelle, R. V., & Lunine, J. I. 1989, Nature, 339, 288